SLIDING MODE CONTROL OF A SOLENOID ACTUATOR FOR SCR SYSTEM

A Thesis

by

Mehmet Polat Küntüz

Submitted to the
Graduate School of Sciences and Engineering
In Partial Fulfillment of the Requirements for
the Degree of

Master of Science

in the
Department of Mechanical Engineering

Özyeğin University
August 2019

SLIDING MODE CONTROL OF A SOLENOID ACTUATOR FOR SCR SYSTEM

Approved by:

Assist. Prof. Dr. Özkan Bebek, Advisor
Department of Mechanical Engineering
Özyeğin University

Assist. Prof. Dr. Barkan Uğurlu,
Department of Mechanical Engineering
Özyeğin University

Assoc. Prof. Dr. Evren Samur
Department of Mechanical Engineering
Boğazici University

Date Approved: 19 August 2019

To my Family.

ABSTRACT

Electromechanical solenoid actuators are widely used in industrial applications that require fast and linear motion. High velocities can be achieved in small stroke lengths consequently the motion results with high-velocity impacts, which may cause excessive noise and create mechanical damage to the parts. In this thesis, the solenoid actuator of a prototype urea injector was controlled with sliding mode control (SMC) to archive soft landing to provide a longer life span to the product. To do that, various test setups were created to understand the urea injector system's behaviors and control them accordingly. Soft landing was achieved with the prototype urea injector while preserving the capability of spraying pressurized fluid.

ÖZETÇE

Elektromekanik sarmal eyleyiciler hızlı ve doğrusal harekete ihtiyaç duyan endüstriyel uygulamalarda sıkça kullanılmaktadır. Kısa mesafede çok yüksek hızlara çıkabilen sarmal bobin pistonu; yüksek güçlü darbeler üreterek, yüksek sese ve parçalar üzerinde mekanik hasara sebep olabilir. Bu tezde, ilk örnek üre enjektörünün eyleyicisi kayan kipli kontrolcü sayesinde yavaş iniş yaptırılarak enjektör sisteminin mekanik ömrünün uzatılması sağlanmıştır. Bunu yapmak içinse bir çok test düzeneği kurulmuş ve üre enjectörü sisteminin davranışları gözlenerek buna göre kontrol edilmesi sağlanmıştır. Enjektör iğnesinin yavaş inişi, enjektörün sprey kapasitesi kaybedilmeden başarılmıştır.

ACKNOWLEDGEMENTS

I cannot express enough thanks to my adviser Dr.Özkan Bebek for providing invaluable guidance and friendship upon this project. I am also extremely grateful for giving me the opportunity to became a member of his research team.

I would also like to thank Dr. Özgür Ertunç for his support as a project leader of this project. My thanks also go to the other members of thesis defense committee, Dr. Barkan Uğurlu and Dr. Evren Samur, for contributing towards finalizing my work with their precious and positive feedback.

Special thanks to my colleagues and employees of the Ozyegin University for made this campus second home to me in my university and master degree adventure that last almost a decade.

Finally I will take this opportunity to thank my family which also own all my successes on this life with their unconditioned love and supports.

This thesis emerges from the needs of TÜBİTAK 1003 project that Ozyegin University and an industrial partner work together. In TÜBİTAK archive project named as Yerli Üre Enjeksiyon Sistemi Geliştirilmesi Ve Motor Testleri and project no designated as 115M093. I was supported by TÜBİTAK since April 2016.

TABLE OF CONTENTS

LIST OF TABLES

LIST OF FIGURES

CHAPTER I

INTRODUCTION

Electromechanical (EM) actuators are replacing pneumatic and hydraulic actuators as they provide more reliable and accurate control, they are more efficient and less hazardous to the environment. Moreover, compactness along with rugged, simple in construction and the lower cost makes them suitable to be used in many domestic and commercial applications which require on and off linear physical movements. The motion of the solenoid actuator is induced by the current supplied to a coil of wire, which then give rise to a magnetic force. Then this force is used to control the motion of the EM actuator.

In the last two decades, many control schemes have been developed to yield higher accuracy for the position control of the electromagnetic solenoid actuator. However, due to the nonlinear behavior of the electromagnetic solenoid actuator, a robust control technique that caters most of the non-linearities is needed so that tracking with high precision may be achieved. So for that reason, different control algorithms can be applied to physical hardware to control the EM solenoid actuator. Besides the precise position control of the EM actuator, another technical problem that should be considered is the high landing impact of the actuator's moving part, known as the plunger or armature, which may cause excessive wear, high noise, and increased actuator's mechanical stress [1, 2]. In addition to the those problems, it will also induce plunger bounce, which may cause uncertainties at the output, leading to poor performance of physical hardware.

The EM actuator has many applications in the various engineering fields. In the automotive industry, most processes are controlled by an EM actuator. For instance,

inside an automatic gearbox drive selectors [3, 4], actuators help the drive selection process. Other applications may include anti-vibration engine mountings [5, 6], air conditioning control [7, 8], locking mechanism [9, 10]. Moreover, they are also used in the agriculture machinery for spraying the chemicals for pest control [11, 12]. In medical EM actuator applications are numerous; they are essential components for the dialysis machines [13, 14], as two solenoids are used to control the blood flow of a person during dialysis. In industrial applications EM actuators are vital components in many of the industrial machines, and they can be found in devices that demand positioning, locking, holding, and rotation. They are also used to control the water pressure in the sprinkler systems and many of such applications [15, 16].

1.1 Selective Catalytic Reduction (SCR) System

Compared to gasoline engines, diesel engines are more efficient and have better emission values in terms of hydrocarbons and carbon monoxide emissions. However, because of the high flame temperature, the nitrogen is oxidized into nitrogen oxide (NO) and nitrogen dioxide (NO_2) which are named commonly as NO_x. The NO_x emission cause ozone depletion, acid rains, and photochemical smog formations. To prevent these, strict regulations have been established to limit the diesel engine NOx emissions [17]. Because of these strict regulations, internal engine control solutions cannot be enough to meet the target emission values. That makes after-treatment solutions necessary. Urea based SCR systems proved itself as a robust solution and have been widely used in diesel engines nowadays. General structure of the SCR system can be seen on Figure 1.

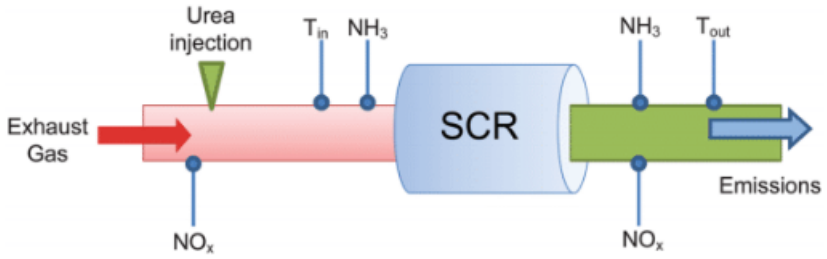

Figure 1: A simplified diagram of an SCR system. The system sprays urea (NH_3) to the exhaust gas to reduce NO_x emissions.

SCR systems use ammonia to chemically consume the NO_x emissions. The ammonia is sprayed in the form of diesel exhaust fluid (DEF), which contains 32.5 percent ammonia and 67.5 percent pure water. DEF is sprayed to the exhaust gases in the catalytic chamber to start a reaction. This reaction can be seen in Figure 2. Technically, more ammonia means fewer NO_x emission but excess ammonia in the chamber may also cause ammonia slip which is the residual of inefficient reaction with NO_x. Because ammonia slip is also harmful to the environment, the ratio between the ammonia and NO_x has to be in accordance with a closed-loop system. Therefore the controlled release of urea according to exhaust emission values is essential to meet the emission standards. At this point urea injectors step in to release the correct amount of urea to clean the exhaust.

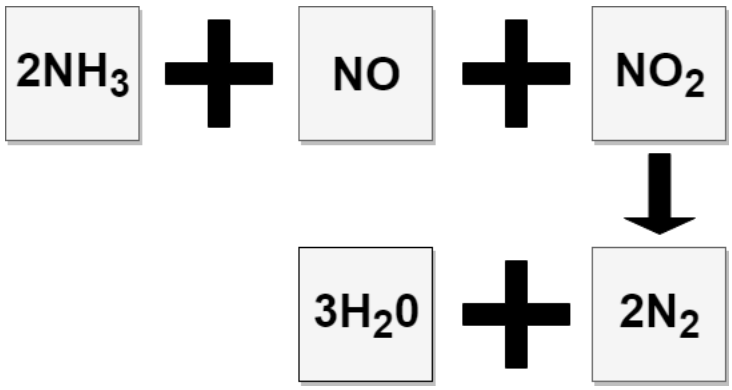

Figure 2: Chemical reaction of NH_3, also known as urea, with NO and NO_2, which are referred as NO_x in automotive industry

1.2 Urea Injector System

The urea injector consists of a solenoid actuator and a needle-type valve that could be opened with actuation. Urea injectors are controlled by engine control units (ECU) and urea spray amount is calculated according to the sensory information collected from the engine and then spray command is given by the ECU to the injector.

In Figure 3, a basic structure of an injector can be seen. The main structure of the injector did not change much within the past years. The system is pressurized by a pump. Then an actuator moves the needle plunger with magnetic force to create a gap between needle seating and needle. This creates a pressure release from the atomizer and then the liquid leaves the injector system as small particles. After injection, a spring moves the needle to its original position.

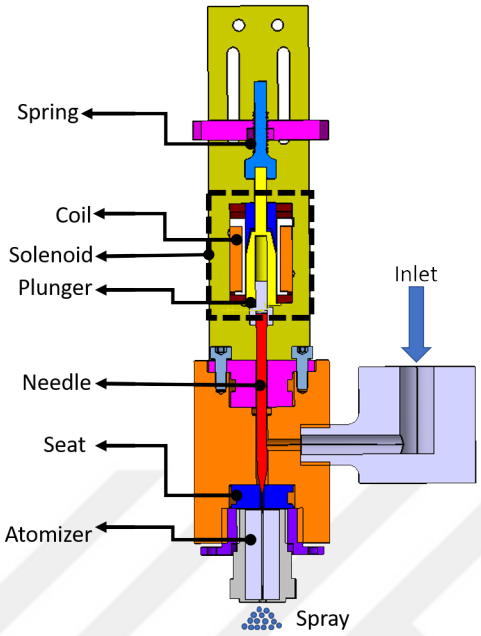

Figure 3: Cut view of an injector system. The solenoid actuator lifts the plunger that is connected to the needle. With this lift, the needle separates from the seating and water is sprayed.

1.3 Soft Landing in Electromagnetic Actuators

The term soft landing [18, 19, 20], also known as soft seating [21], refers to the EM actuators slow-closing process. When energized, the EM actuator stores the kinetic energy in the spring, which is then released when the EM actuator is inactivated. The elastic energy stored in the spring accelerates the motion which causes the high landing velocity. This causes high-velocity impact and problems associated with it. To overcome this problem, seating velocity can be reduced with control algorithms, hence the soft landing of the EM actuator is achieved. This phenomenon is very useful to increase the life of the mechanical parts, and it has been used in many applications like electromagnetic internal combustion engine valves [22, 23].

1.4 Thesis Contribution

This thesis aims to create an closed-loop controlled robust soft seating system that works with any solenoid actuator. The control system slowed down the mechanical parts before impact so the solenoid actuators could be quieter and can work longer. Although solenoid actuators have a wide area of use, the specific case that is included in this thesis is the soft landing for a urea injector system. The experiments were conducted on a prototype urea injector that was designed for a new SCR system. Creating a robust controller for the custom-designed device required many tests and those tests required new test setups. New test setups that were created for this thesis can be used for the development of other injectors in the future. With the experiences gained from the hardware setup, a model for the non-linear solenoid actuator was created. The model can shorten research time by eliminating the time that is spent to create test setups for simple experiments.

1.5 Thesis Outline

In this thesis, a soft landing control method for a urea injector was designed. This thesis provides five chapters. Chapter 1. Section 1.1 introduces electromagnetic actuators and brief literature review. Section 1.2 presents the Selective Catalytic Reduction (SCR) system to make it familiar for further chapters because the urea injector that design on this thesis will be a part of the SCR system. Section 1.3 is about how injectors work and why we need soft-landing. Section 1.4 introduces the soft landing process which is the main quest of the thesis. Chapter 2 is about creating a simulation of the solenoid actuator. Because of solenoid actuators are highly nonlinear, creating a model needs to be more precise. Physical and magnetic structure of the simulations and the equations given in this chapter. Moreover studies about taking correct parameters for simulation and the setups for this are shown. With the creation of the experimental test setup for soft-landing and the comparison

of the simulation result, this chapter is concluded. A study about Sliding Mode Control is given in Chapter 3. The experimental results from the test setup that was mentioned in Chapter 2 for soft-landing with SMC and PID controller was also shown in this chapter. This chapter also demonstrates the robustness of SMC and why it was used for further soft landing test in this thesis. In Chapter 4, an observation about OEM injector and how the information from that observation was used for injector tests were discussed. After a short design phase for prototype injector for soft landing tests, pressured fluid test for OEM and later prototype injector with soft landing have included in this chapter. Finally in chapter five, conclusion of the thesis is given.

CHAPTER II

MODELLING OF A SOLENOID ACTUATOR

In this chapter, the efforts for finding correct parameter values and the workings of the simulation is explained. The simulations used for tuning controllers mentioned in Chapter 3. Matlab's Simulink was chosen as the model development environment. A solenoid actuator model was created and an effective controller was tuned using the model.

2.1 Simulation

To understand the behavior of the solenoid actuator, a simulation model was created in Matlab, Simulink. To obtain reliable results, the characteristics of the modeled device must be precisely determined. Therefore, studies were carried out by using close to realistic parameters.

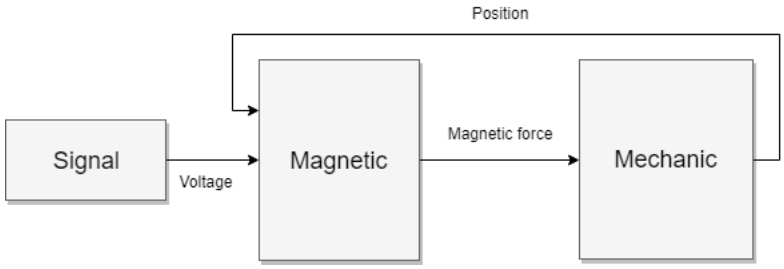

Figure 4: The basic structure of the solenoid model. The two physical subsystems, magnetic and mechanic, are modeled separately

Figure 4 shows the two main parts of the simulation. These parts are magnetic (Figure 5) and mechanical parts (Figure 6). While magnetic part calculates the magnetic force and current with applying voltage, the mechanical part's output calculates how the piston moves with the generated magnetic force.

In the magnetic part , Faraday's equations were used to find the magnetic flux. According to Faraday's law, the flux is equal to the voltage divided by the total number of turns of the coil as in (1).

$$d\phi/dt = (V - iR)/N \tag{1}$$

In (1) ϕ is the flux, V is the voltage, R is the resistance of solenoid coil, N is the turn number of coil. To find the flux density, the flux is divided into the cross-sectional area of the coil as in (2).

$$B = \phi/A \tag{2}$$

In (2) B is the flux density, A is the cross-sectional area of the coil.

The flux density is used to find the magnetic force and magnetomotive force after this point. The magnetic force can be found by squaring flux density times cross-sectional area of the plunger divided by twice the magnetic permeability constant of the flux density core as in (3).

$$F_{mag} = (A \cdot B^2)/(2 \cdot \mu_0) \tag{3}$$

In (3) the F_{mag} is the magnetic force, μ_0 is the magnetic permeability constant of the flux density core.

Magnetomotive force is found by multiplying the magnetic field density by the distance of the magnetic field. To find the density of the magnetic field generated in the air, the flux density is divided by the permeability constant of the air (4).

$$H_{air} = B/\mu_0 \tag{4}$$

In (4) the H_{air} is the density of the magnetic field generated in the air.

For steel, permeability is not constant, but it can be represented as a function of the B-H curve. A look-up table for 430 steel [24] was used in our simulations (5).

$$H_{steel} = f(B) \tag{5}$$

In (5) the H_{steel} is the density of the magnetic field generated in the steel, $f(B)$ is the magnetic field density equation of 430 steel.

Magnetomotive forces, which are formed by air and steel, are founded by the sum of permeability of air multiply with length of the stroke and permeability of steel multiply with the length of the steel section affected by the magnetic field (6).

$$F_{MM} = H_{air}s + H_{steel}L_{steel} \tag{6}$$

In (6) the F_{MM} is the magnetomotive force, H_{air} is the density of the magnetic field generated in the air, H_{steel} is the density of the magnetic field generated in the steel, s is stroke or the total distance that plunger can move, L_{steel} is the length of the steel section affected by the magnetic field. The coil current can be founded by magnetomotive force divided by number of turns that coil has, as in (7).

$$i = \frac{F_{MM}}{N} \tag{7}$$

In (7) i is the coil current.

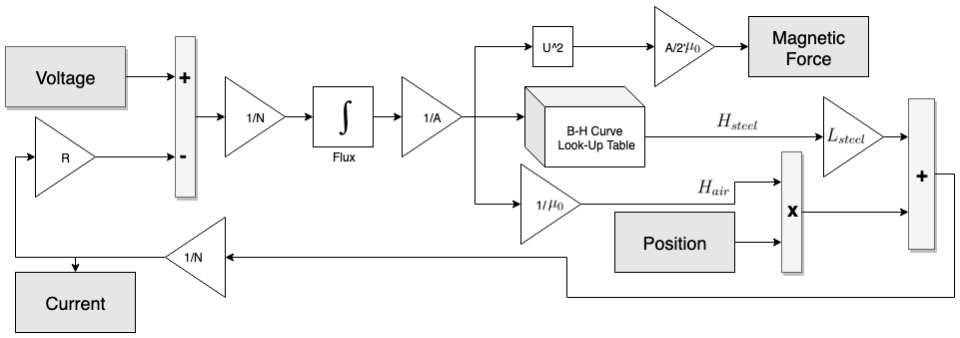

Figure 5: Magnetic structure of the simulation. A flow chart representing the Simulink model is given here.

The total force acting on the piston is found by adding magnetic force which is found in the magnetic part and the force of the spring and friction (Figure 6). Since the multiplication of mass with acceleration is equal to the force, the acceleration can be found by dividing force with mass. The integral of the acceleration will give the velocity, the integral of the velocity will give the position. When the velocity is multiplied by the friction coefficient and the position is multiplied by the spring constant, the mechanical forces acting on the plunger are found.

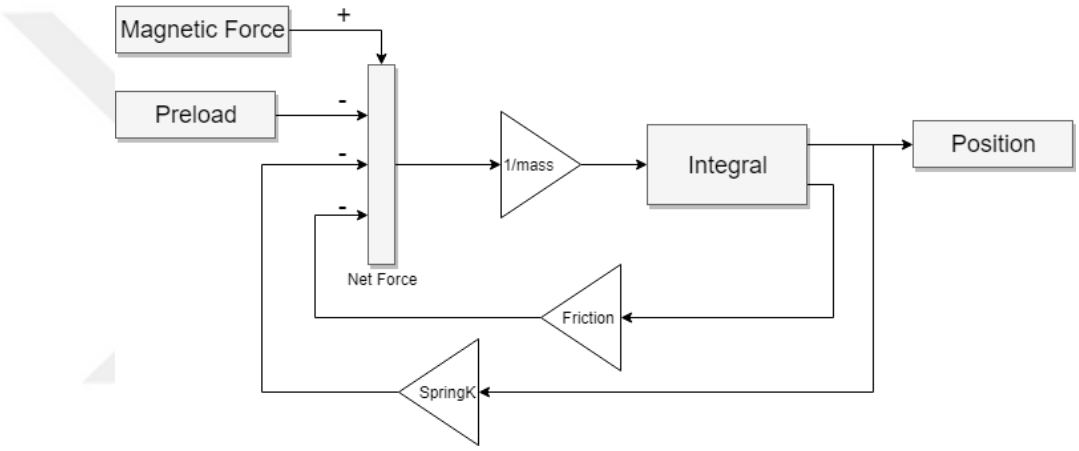

Figure 6: Structure for the mechanical part of the simulation. Simulink model is simplified and a flow chart version is provided here.

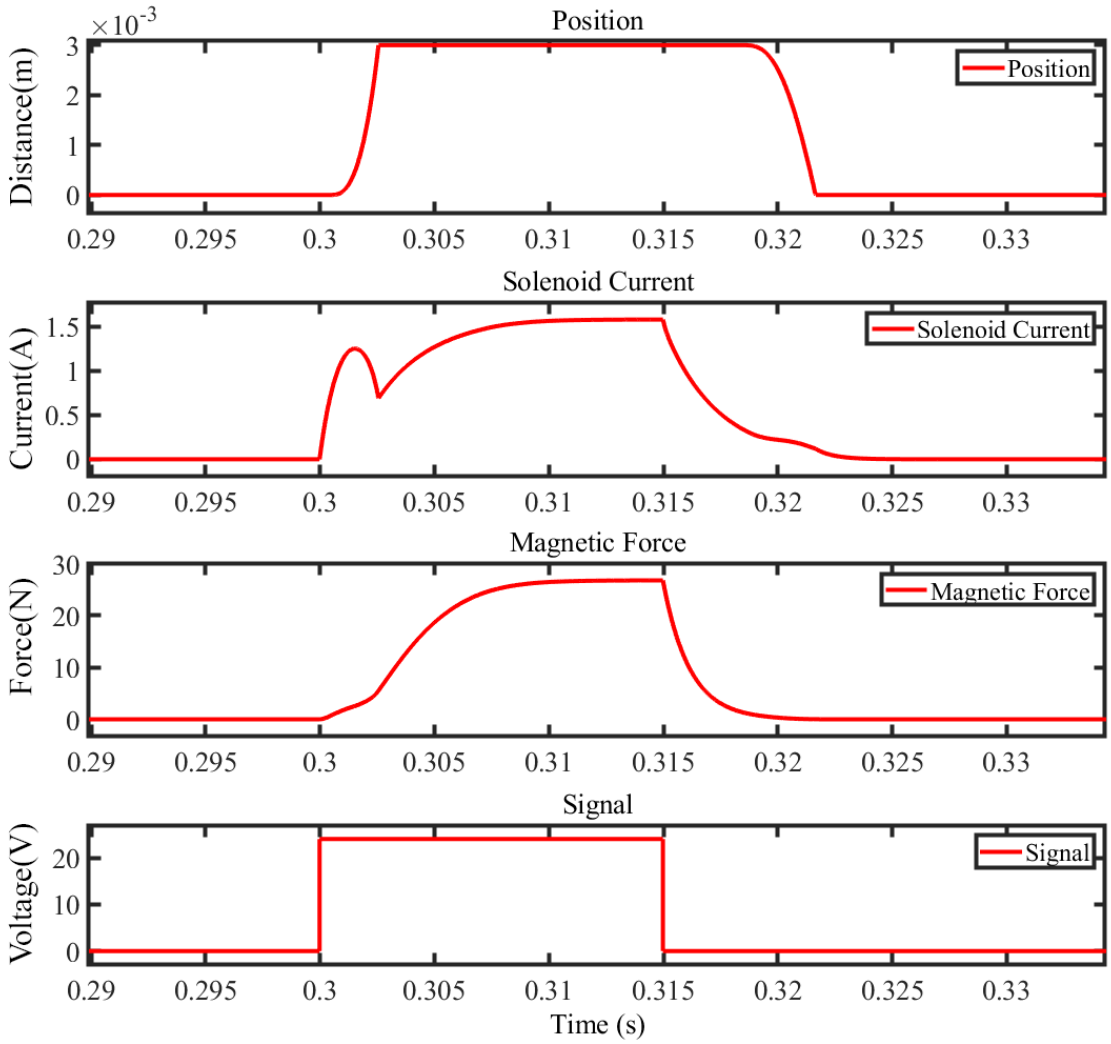

Figure 7: Solenoid actuator simulation results. From above to below; position, current, magnetic force and voltage

2.1.1 Model Parameters Identification

To verify the link between test results and simulation results, the physical properties of the hardware has to be found. According to the simulation, only the spring coefficient and B-H curve of the metal are needed. To determine spring force coefficient, a load cell (FUTEC LBS200) was used (setup is shown in Figure 8) and results show that the springs are mostly linear. Spring coefficient of a linear model can be calculated easily (Figure 9). The magnetic force of the solenoid actuators was also measured with the

load cell to compare with simulation results. Furthermore, stroke length, maximum current values used by actuator and opening and closing time of the actuator were found to compare.

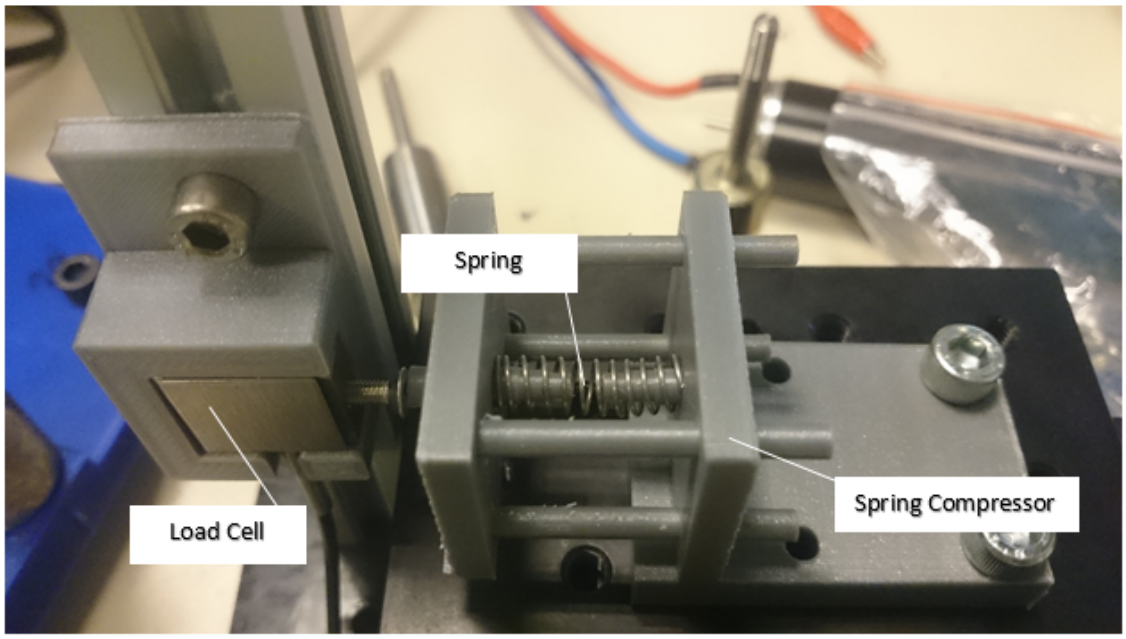

Figure 8: Test setup for finding spring coefficient. Load cell collects data from the compressed spring.

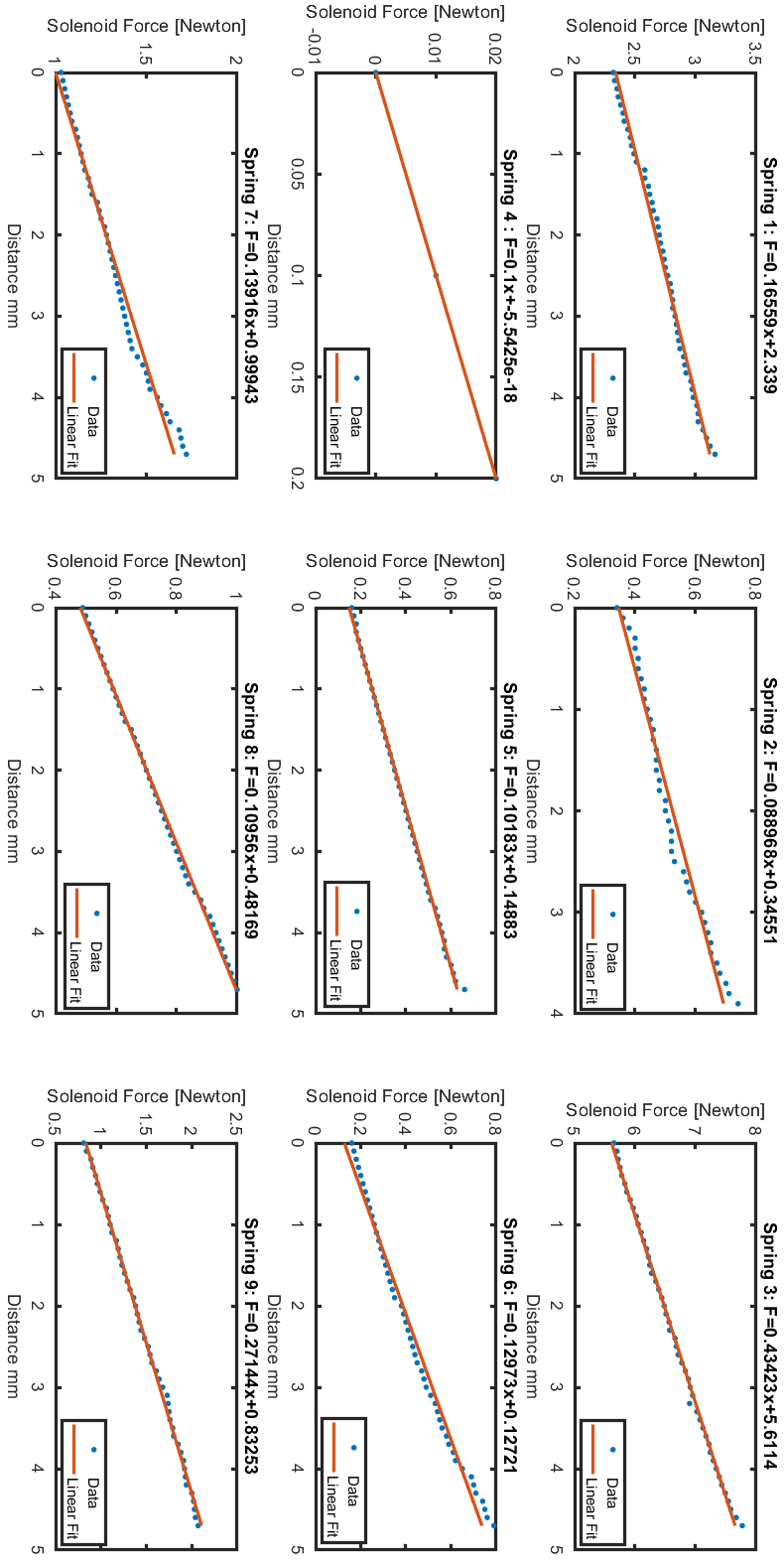

Figure 9: Test results for used springs.

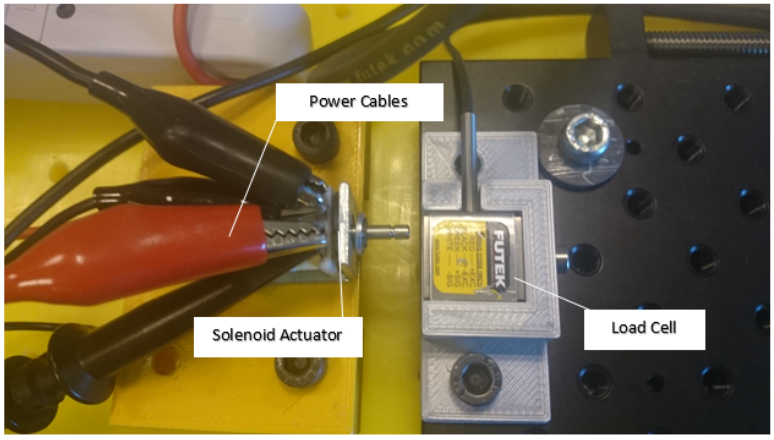

Figure 10: Test setup for measuring solenoid force

The solenoid actuator's nonlinear force outputs require multiple measurement for different stroke lengths. EM actuator's force outputs reach maximum when the plunger about to close. Those nonlinear force outputs can be seen on Figure 11.

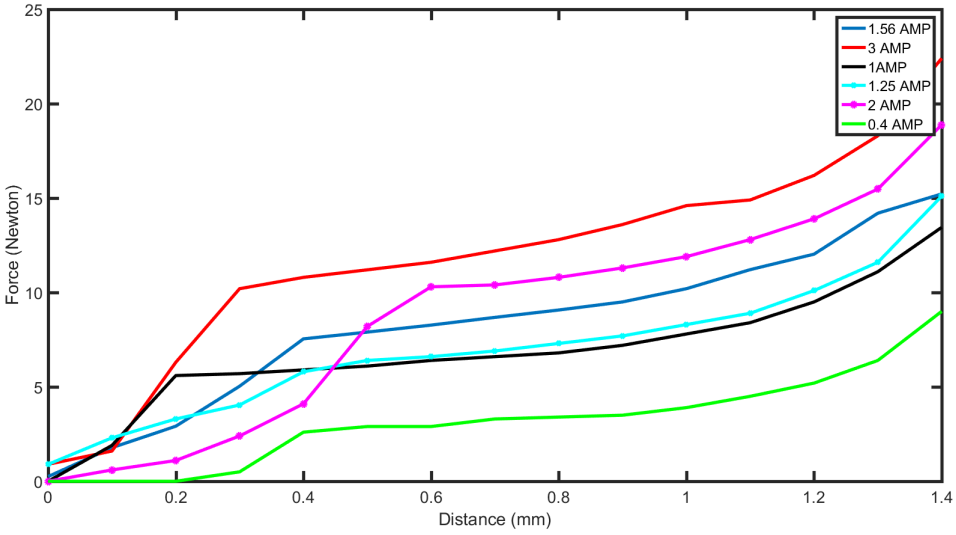

Figure 11: Test results for different solenoid actuators. Load cell collect data from the powered solenoid actuator.

2.2 Forming the Test Setup

2.2.1 Experimental Setup for Softlanding

The main scenario in the experiment was to focus on the solenoid actuators that are commonly used in industrial production lines or the automotive industry. For that reason, a controller which has capability similar to a high-speed digital control device, that is used in industrial applications such as ECU or PLC, was used.

Both the PID and the Sliding mode controllers were implemented on a digital computer, which consists of feedback and apex seeking algorithm that ensure the tracking of position concerning the desired input signal. Various reference signals are designed to make sure that soft landing of the EM actuator to achieve lower velocities at the time of closing. The experimental setup was designed to control a mainstream 24 V solenoid actuator. A Quanser Q8 USB data acquisition (DAQ) system was used with Matlab Simulink to implement the digital controllers and generate 16-bit analog output control signals. Since the DAQ board operates on low voltages and low currents, the output of the control algorithm was then sent to a 12-bit analog input module (NI9201) attached to a NI CompactRIO Controller. The analog input module reads the control signal and converts it to a PWM signal in the Labview software. Then a digital I/O module (NI9472) fed the solenoid actuator with the generated 24 V PWM signal. A current and voltage data were recorded using a Keysight DSOX2004a oscilloscope with a Keysight 1146B current probe and a generic voltage measurement probe. The motion of the plunger was measured using a Broadcom HEDS5645-I13 encoder which was fitted with a tendon-capstan mechanism to convert the linear motion of the plunger to angular motion. The encoder has two 90° phased channels and with quadrature reading it can provide 2048 counts per revolution resolution, which would provide 18.36 μm linear resolution.

The flowchart of the overall control process is given in Figure 12. This control scheme will also be used in further tests.

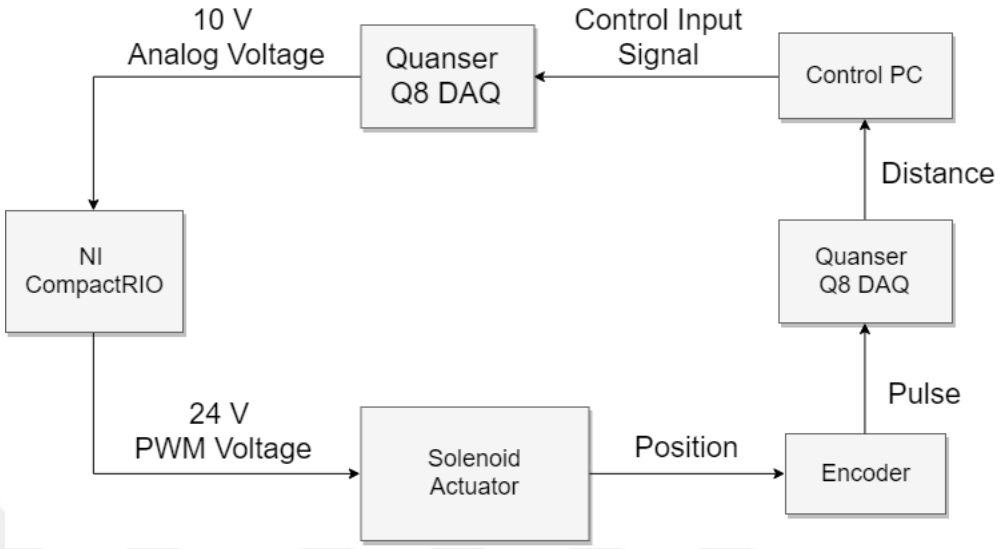

Figure 12: Flowchart of the closed loop position control process.

Parameters of the solenoid that used for experiments can be seen in Table 1

Plunger Mass	Spring Ceofficient	Coil Resistance	Coil Turns
91.32 g	420 N/m	46.1 Ohm	2900

Table 1: Plunger mass, spring coefficient, coil resistance and coil turns of the solenoid actuator that was used for experiment. Parameters are provided by the manufacturer.

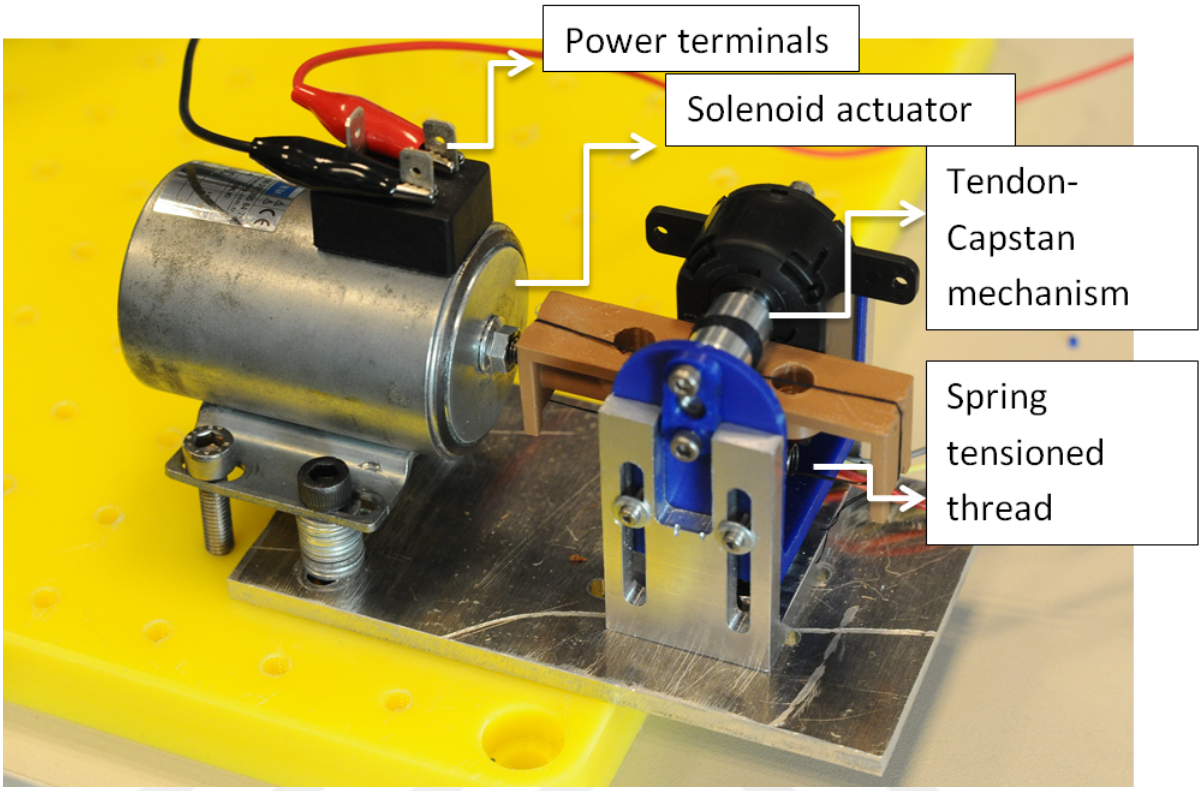

Figure 13: A test setup for soft landing experiments

Simulation and test setup opening time comparison with On-Off control can be seen in Figure 14.

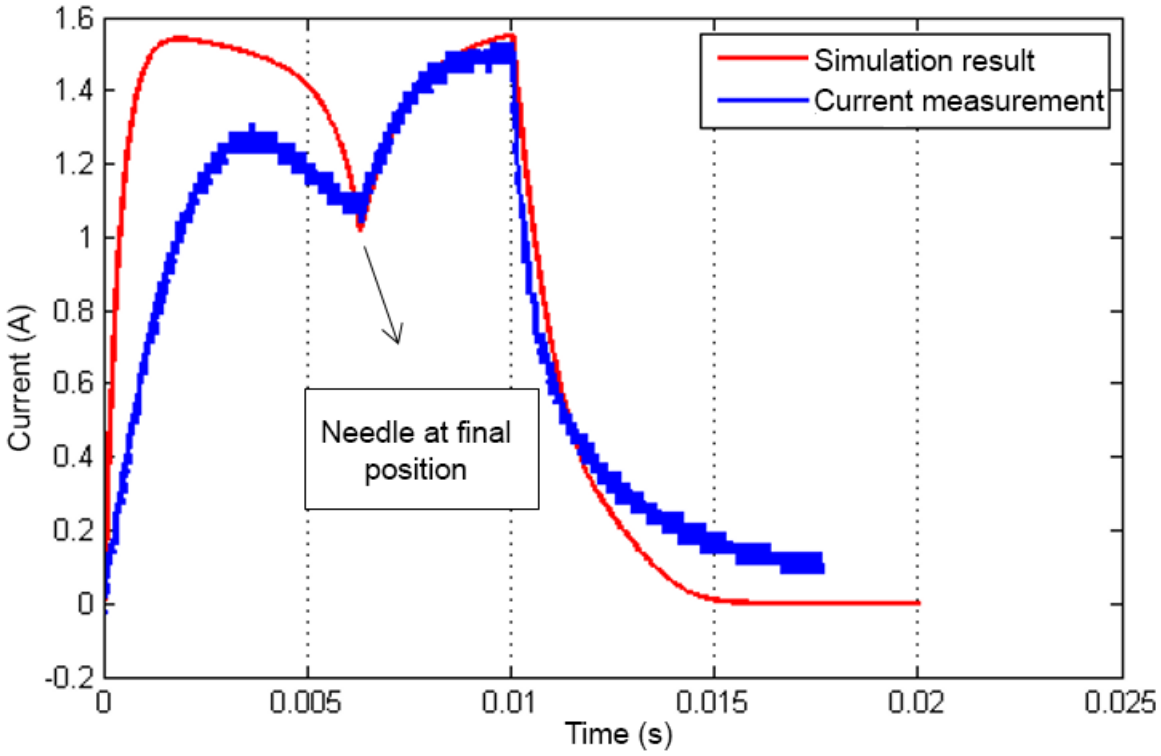

Figure 14: The figure shows that the opening time of the experiment result is very close to the simulation results

CHAPTER III

SOFT LANDING TEST RESULTS

In this chapter, performance of the different controllers to achieve soft landing are demonstrated via experiments. The test setup that was described in Chapter 2 was used in experiments.

3.1 Control Methods

To achieve soft landing, two types of controllers with a position feedback was used. They are Proportional Integral Derivative (PID) and Sliding Mode Control (SMC). The reason for using those controllers is the need for a controlled plunger movement before impact happens. The timing is very important for accurate spraying however to reduce the damage, the plunger should be slowed down before impact. Therefore a simple on-off control cannot be used to achieve soft landing. Controlled movement of the plunger is provided by optimized position profiles that are applied by a closed-loop controller with a position feedback. The control law aims to make the output position y to track the desired position profile y_{des}, and for that, it is required to make the error, e as given in (8), approaches to zero.

$$e = y_{des} - y. \tag{8}$$

3.1.1 PID Control

Proportional Integral Derivative (PID) controller is the most commonly used controller in industrial control systems involving feedback. The controlled output is adjusted depending on the present error [25].

A digital PID controller was implemented at 1 kHz sampling rate as in (9) where T_s is the sampling rate, and k_p, k_i, and k_d, are proportional, integral and derivative

control constants, respectively.

$$F(z) = k_p E(z) + k_i \frac{T_s}{2} \frac{z+1}{z-1} E(z) + k_d \frac{z-1}{zT_s} E(z) \tag{9}$$

3.1.2 Sliding Mode Control

Practical application of the control law on the actual plant and the simulated model may differ in the results because of the parasitic or un-modeled dynamics of the system or the external disturbances faced by the actual plant or the parameter uncertainties.

Sliding Mode Control (SMC) is a very effective method to compensate the parameter perturbations in the systems [26]. Moreover, it is also very robust to the matched uncertainties of the system, for instance, the uncertainties that enter the system at the point of inputs [27].

The sliding mode control algorithm works on a two-step approach to control the system i.e. designing of sliding surface and the designing of the control input [28]. The first step of implementing the algorithm is to define a sliding surface σ upon which the system trajectories are forced to slide, so for that, the sliding surface is defined as (10).

$$\sigma = \frac{de}{dt} + ae \tag{10}$$

where parameter a is an arbitrary positive constant that determines the position of the unique pole of reduced dynamics of the system when the system is sliding. As the trajectories of the system reach the sliding surface or sliding manifold, the system does not require model parameters.

The successive step is to find a control action that keeps the system trajectories onto the sliding manifold or to steer the sliding manifold variable σ to zero. As the trajectories of the system reach the sliding surface or sliding manifold the control law ensures that they stay there forever. Despite the control law effort, a phenomenon known as Chattering may occur, which as a result, may excite the unwanted dynamics of the system and is sometimes very undesirable in the case of underactuated systems.

Thus the control law u can be defined for the system as:

$$u = -U \cdot sat(\sigma) \tag{11}$$

where,

$$u = \begin{cases} -U, & \sigma < 0 \\ U, & \sigma > 0 \end{cases}$$

Here, U is arbitrarily chosen large positive constant, which is to be tuned until the desired output is achieved. Continuing with the Full-State Stabilization of the solenoid actuator, and interpreting the error dynamics stated in (8). By doing the Lyapunov analysis one would get,

$$\frac{dv(e)}{dt} = e \cdot \frac{de}{dt} = e(y_{des} - y) \tag{12}$$

Hence, the error can be stablized by controlling y_{des} as,

$$y_{des} = \frac{dy}{dt} + ae. \tag{13}$$

Moreover the sliding surface will be of the form as,

$$S_\sigma = y_{des} - \frac{dy}{dt} - ae. \tag{14}$$

For the states to stay on the sliding manifold the below condition should be met

$$\sigma \cdot \frac{d\sigma}{dt} < 0 \tag{15}$$

The main control target of the sliding mode control is to move the system state onto the sliding surface, i.e. $S_\sigma = 0$.

3.1.3 Reference Signal for Soft Landing

Figure 15 shows the baseline performance of the solenoid actuator with simple on/off control, having a 2-second-long on-time, and closing power at the 2-second mark. A delay can be seen in the motion of the actuator, which is due to the residual magnetism stored in the plunger of EM actuator.

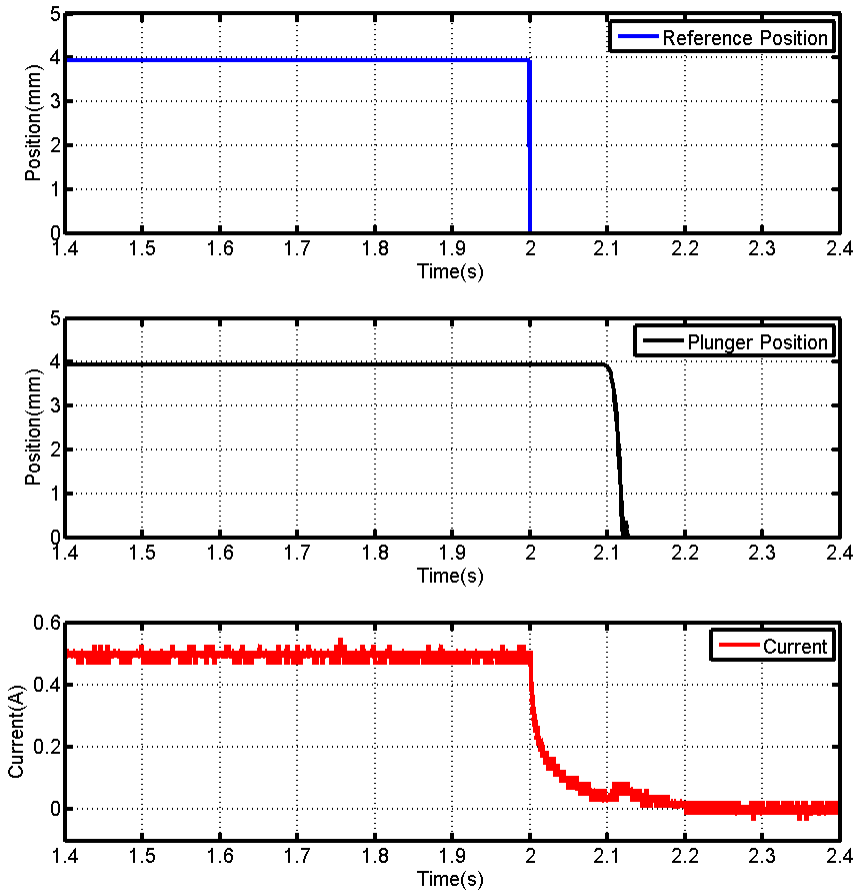

Figure 15: Baseline performance of the solenoid actuator with on/off control: The opening characteristics for all reference signals are same and are not shown in the figures. The plots above capture the closing of the solenoid actuator. When the top and the middle plots are compared, the lag of the plunger position is visible. The delay is due to the residual magnetic force kept in the solenoid after the input is turned off. The plunger starts its motion when the spring force overcomes the magnetic force. The peak seen in the current plot (around 2.1 s) during the closing is due to the eddy current effect.

Figure 16 shows the used three different reference profiles created to achieve the soft landing. The robustness of the control algorithms was tested using the reference profiles. All the signals were created to achieve the soft landing of the EM actuator, where signal 3 is approximated by a cubic polynomial, while signal 2 and signal 3

are approximated by lines. Signal 2 has a closing time of 0.5 s and the signal 1 has a closing time of 0.2 s, as depicted. The opening profiles of all the reference signals used are same and are not shown in the figures.

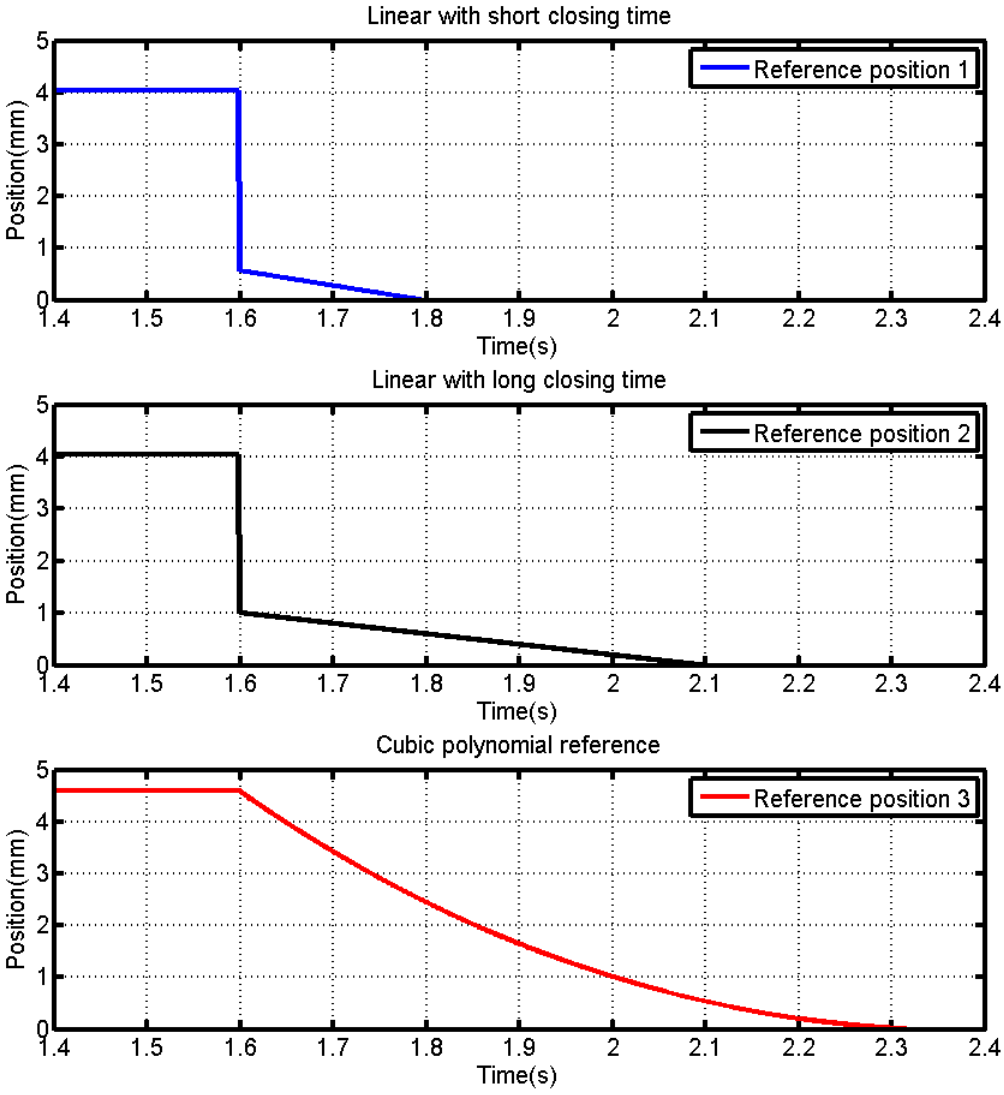

Figure 16: Reference position signals generated to compare the control algorithms applied: The top plot is the first reference signal, where the soft landing phase is 0.2-seconds-long. The middle plot is the second reference, where the soft landing phase is 0.5-seconds-long. The bottom plot is the third reference signal, where the soft landing phase is formed using a cubic polynomial and is 0.7-seconds-long.

3.1.4 Results of the Closed Loop Position Control

Closed loop position tracking was achieved in the real-time,, using both control algorithms. Encoder data in the form of a linear position was feedback to the controller, according to which the control effort is applied by the respective controller to track the reference input. The tracking results are shown in Fig. 17. RMS position tracking errors are given in Table 2. SMC has considerably smaller error compared to PID. Furthermore the Figure 17 shows the performance of SMC over the PID controller, as the SMC tracks the position profile of the different input signals with less error and considerably better tracking history.

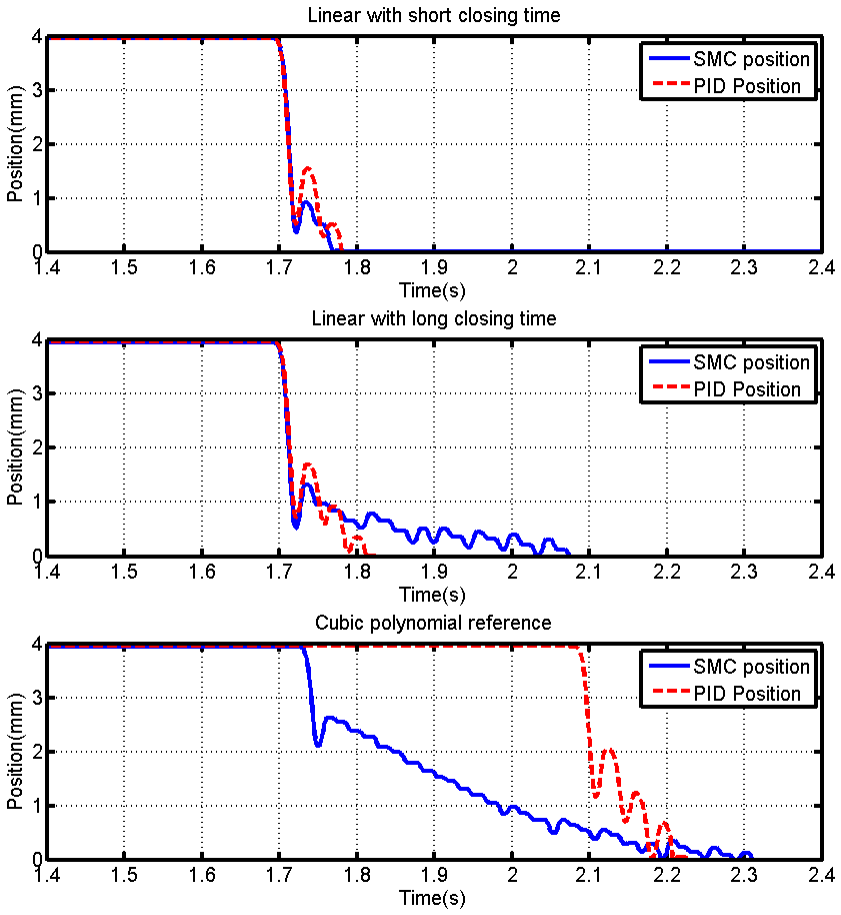

Figure 17: Position outputs for each the three reference signals. Compared to the response of the On/Off control shown in Figure 15 the plunger motion is either delayed or softened. In all cases, PID control has poor tracking performance.

Table 2: RMS values of position tracking errors.

RMS values of the Plunger Position (mm)			
Controller	1st Ref Signal	2nd Ref Signal	3rd Ref Signal
PID	0.527	0.498	1.900
SMC	0.482	0.394	0.238

Experiments were repeated 10 times, here the average of the RMS values is reported.

3.1.5 Power Consumption

Soft landing application does not guarantee power reduction, in fact, it can increase the energy consumption since more energy would be required to slow down the plunger. The aim of soft landing algorithms is to increase the lifespan of the mechanical parts. This increased energy consumption can be observed in the Table 3 for different reference signals. This increase is also evident from the Figure 18, as the PID consumes more energy than the SMC controller because the control signal generated by the PID controller tracks the input signal less efficiently and for that, the energy requirement decreases.

In Figure 18 current measurements for the three reference signals are shown.

Charge (Coulombs)			
Controller	Reference 1	Reference 2	Reference 3
PID	5.32	5.40	7.31
SMC	5.45	6.05	6.50

Table 3: Current Dissipation

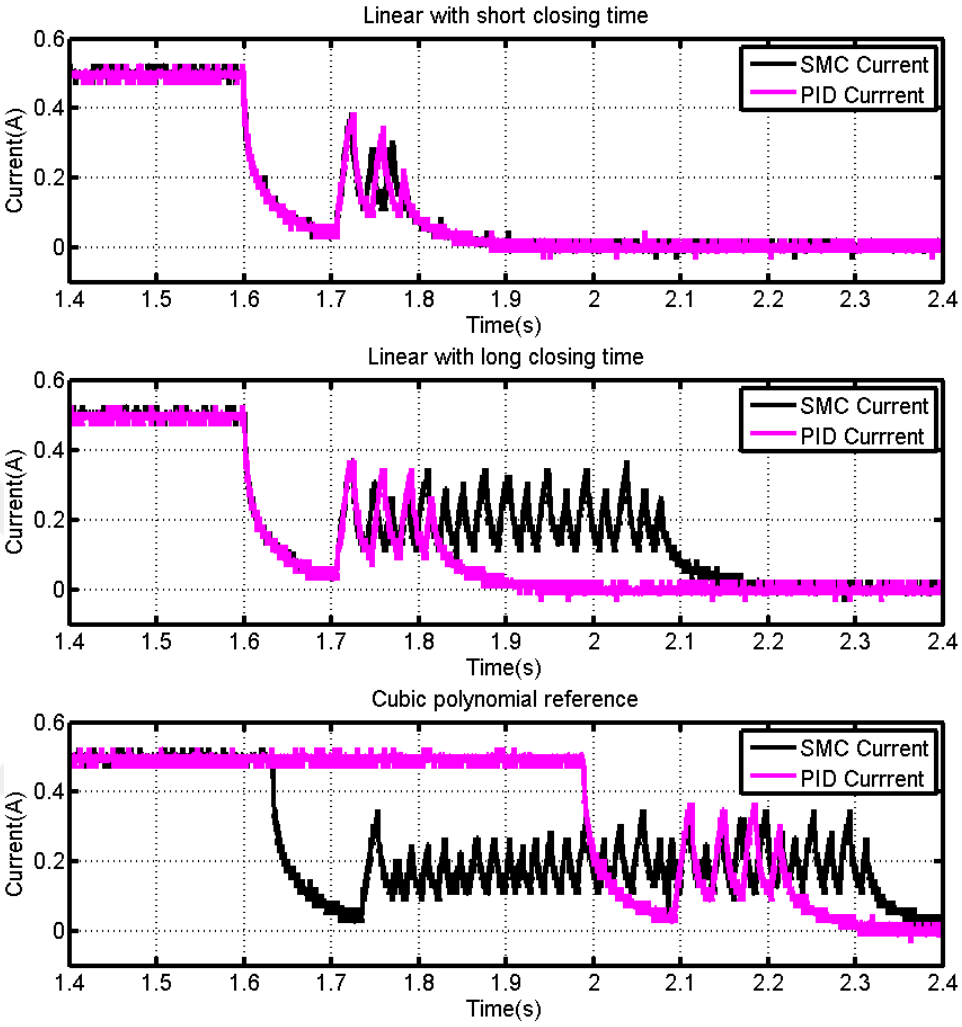

Figure 18: Current output measurements for the three reference signals. The top plot shows the current profiles of the controllers for the short soft-landing reference. The middle plot shows the profiles for the longer soft-landing reference. The PID controller cannot hold the position and lands prematurely. In the bottom plot, current profiles for the cubic polynomial reference signal are shown. The PID controller is less responsive to the slow changing reference signal.

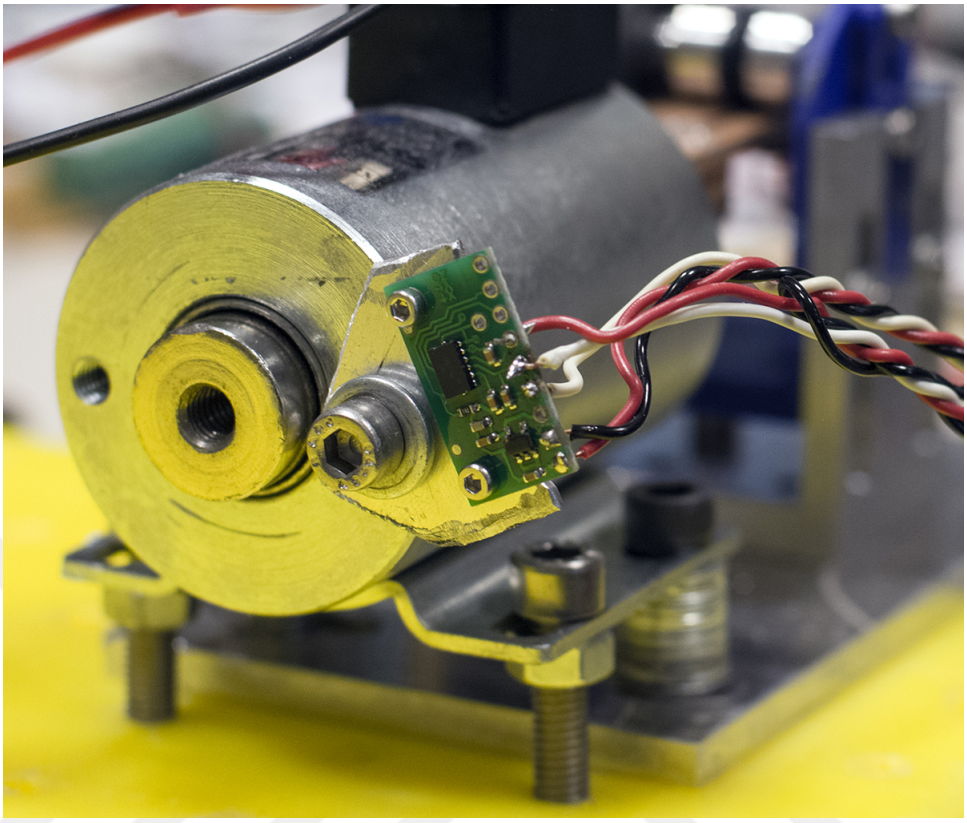

Figure 19: An accelerometer is attached to the body of the solenoid actuator, to predict the magnitude of impact by measuring the acceleration caused by the plunger at the time of closing.

3.1.6 Soft Landing and the Magnitude of Impact Velocity

In this particular scenario, closing impact of the plunger should be as slow as possible for the long lifespan of the mechanical parts of the EM actuator. The indicators that define the soft landing are holding force and the closing velocity. The closing velocities for different reference profiles were calculated for the PID and SMC controllers and results are shown in Table 4. For all reference signals, the SMC shows low closing velocities for the plunger. Evidently, the Reference Signal 3 has the lowest impact velocity due to its cubic closing profile.

It is evident from the Table 4 that for the same input signal profile the seating velocity for the SMC controller over performs the PID controller.

Table 4: Comparison of Plunger Closing Velocities and Impact Accelerations for three different reference signal profiles. Experiments were repeated 10 times, here the mean and standard deviation ($\sigma \pm \mu$) of the measurements are reported.

		Plunger Closing Velocity (mm/s)	**Impact Acceleration (g)**
On/Off control		15.8	1.487
Ref 1	PID	11.0±1.280	1.369±0.246
	SMC	7.07±1.470	1.400 ± 0.421
Ref 2	PID	8.14±1.420	0.938±0.185
	SMC	6.28±0.811	0.392±0.0695
Ref 3	PID	9.00±1.800	1.146±0.169
	SMC	6.55±0.749	0.483±0.0825

A Freescale MMA7361LC 3-Axis Accelerometer was attached to the body of the solenoid actuator to measure the impact caused by the plunger (see Fig. 22). In Table 4 the measured maximum acceleration values are reported. The minimum acceleration is measured when the reference signal 2 is followed using SMC. This result shows that there is an optimal closing time to achieve minimum impact created by the plunger.

Box plot representations of RMS values, plunger closing velocities and impact acceleration data can be seen on Figure 20,21 and 22.

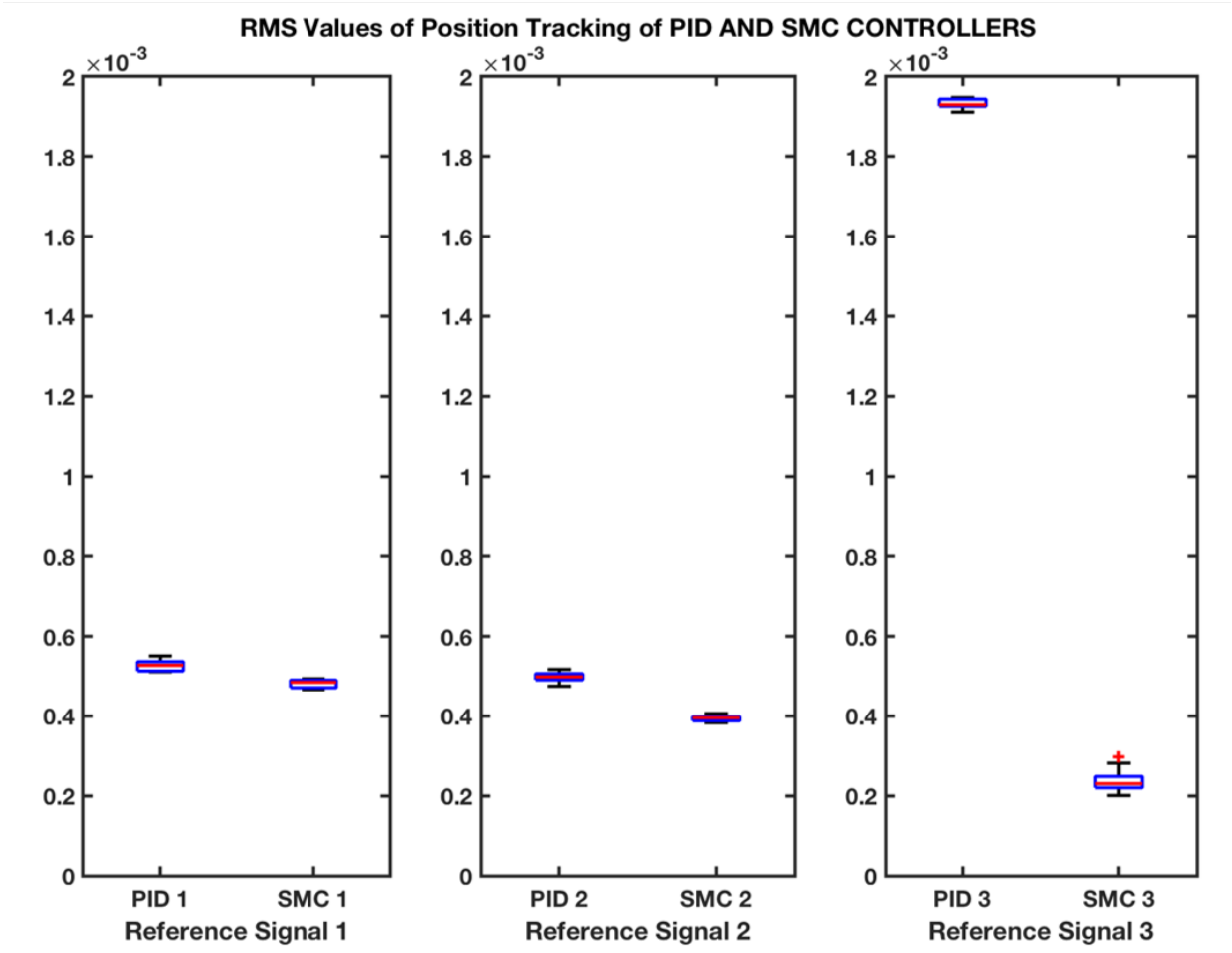

Figure 20: Tracking error of three different signal can bee seen with corresponding controller

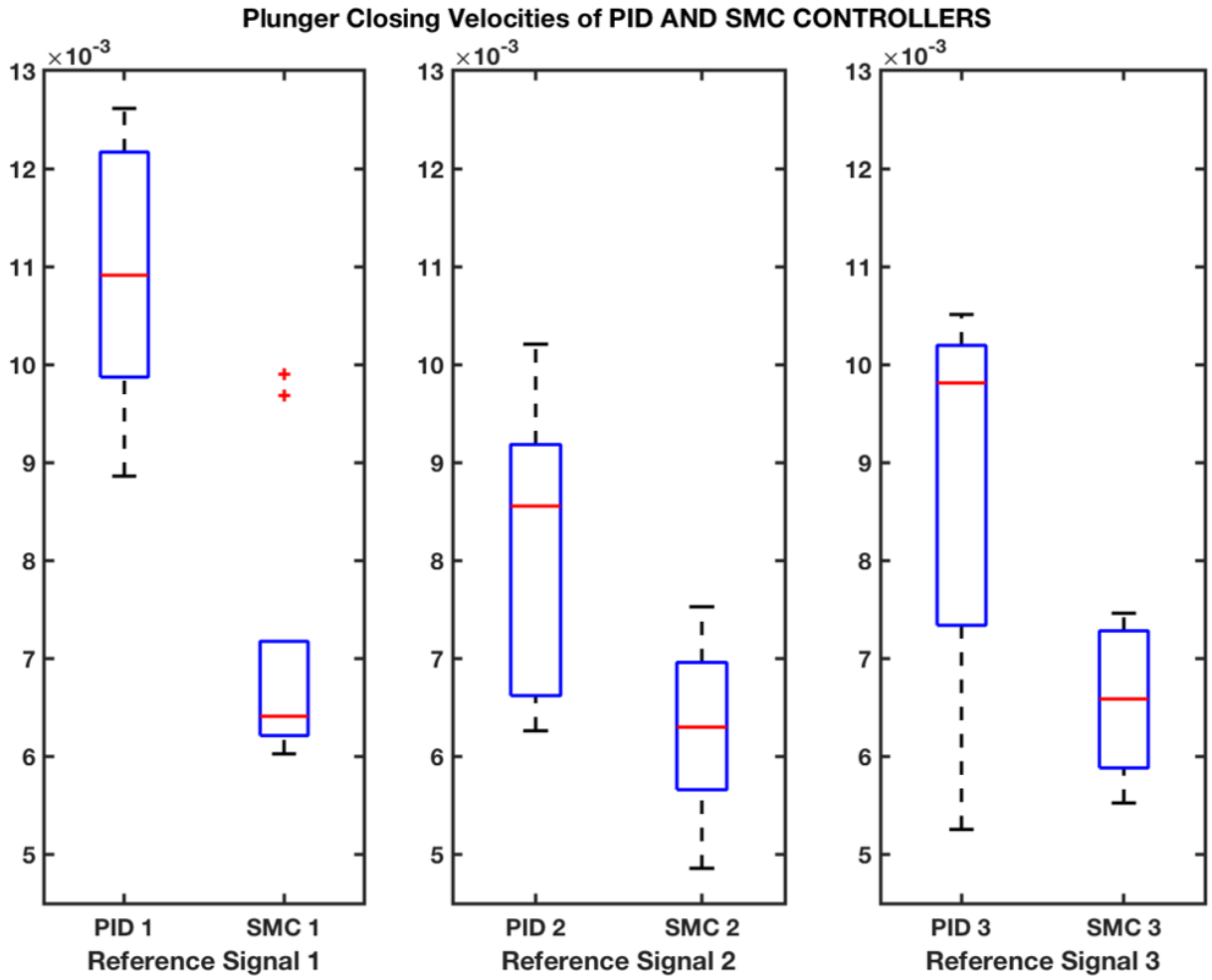

Figure 21: Closing velocities of three different signal can be seen with corresponding controller

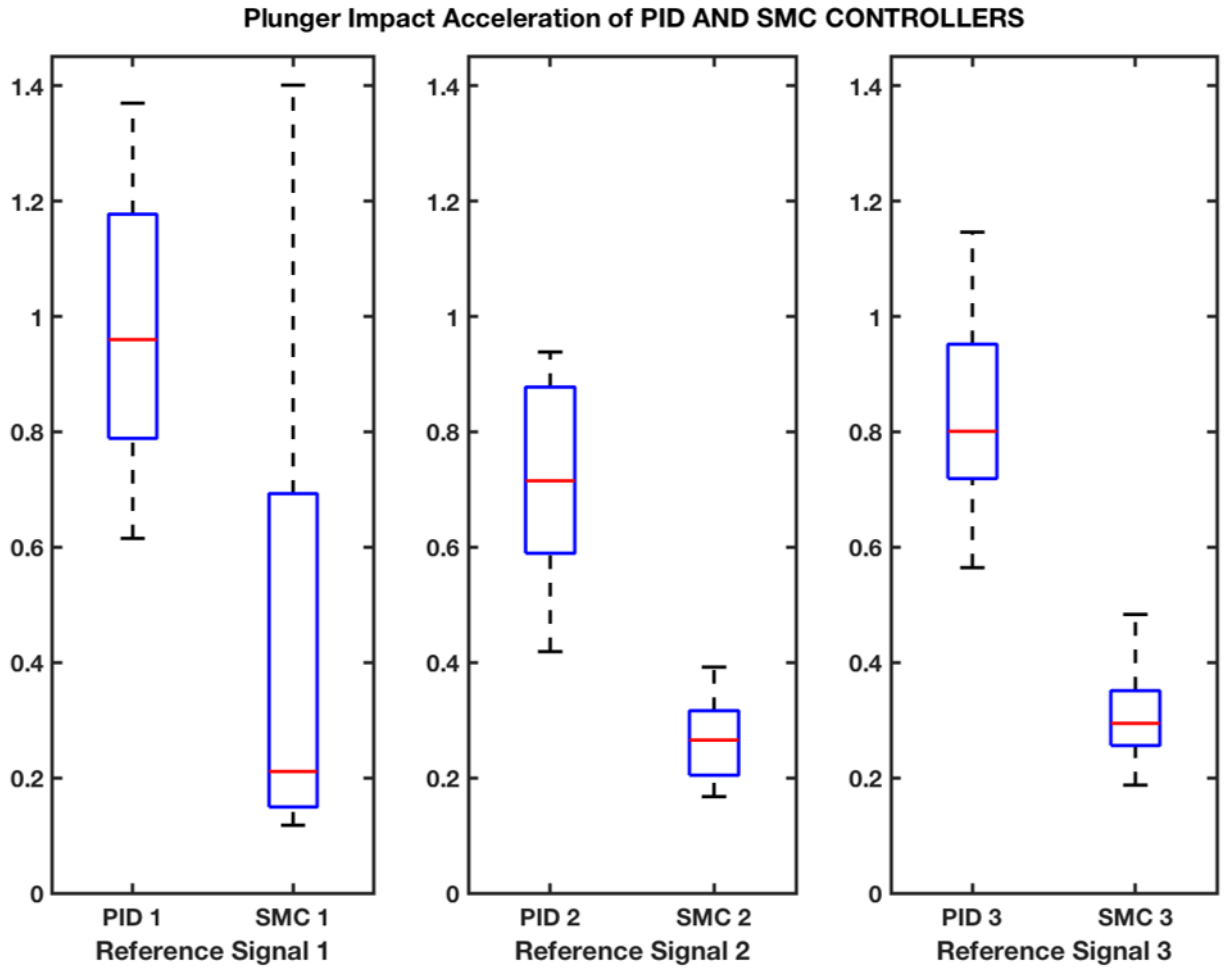

Figure 22: impact acceleration of three different signal can be seen with corresponding controller

CHAPTER IV

INJECTOR TEST SETUP

4.1 Observations from an OEM Urea Injector

A common Original Equipment Manufacturer (OEM) urea injector compared to the prototype that is produced in the research lab. The OEM injector is cut half to understand its inner structure. The cut injector can be seen in Figure 23. Several tests were made on these injectors. Mainly opening and closing times, current and voltage usage profiles, and latency between needle motion and actuation signal, needle movement, and liquid release tests were conducted. The first two could be obtained using oscilloscopes, but finding the latency between the actuation signal and fluid release is challenging since liquid release could only be observed visually. Therefore the spray room test setup (Shown in Figure 24) of the Fluid Dynamics and Spray Laboratory was used to conduct latency tests.

Figure 23: Common urea injector cut with water jet for observation of its internal structure.

To catch the instance when the liquid release starts, a high-speed camera was placed to observe the spray cone created by the injector. Behind the spray cone and in high-speed camera's sight an LED was placed. Injector power signal was connected in parallel to the LED to synchronize high-speed camera and opening signal. Then in slow motion, the time between LED's glow and liquid release was recorded. High speed video's frame number was counted and latency was determined (Figure 25).

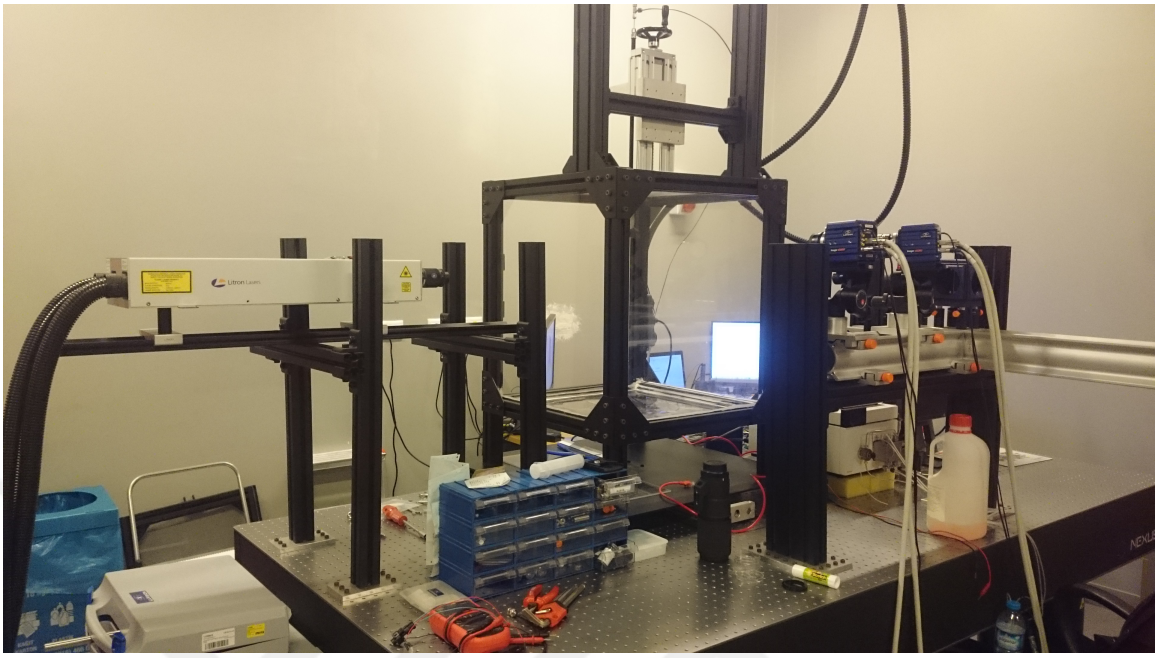

Figure 24: Test setup for injectors with high speed cameras and fluid pumps for spray observation

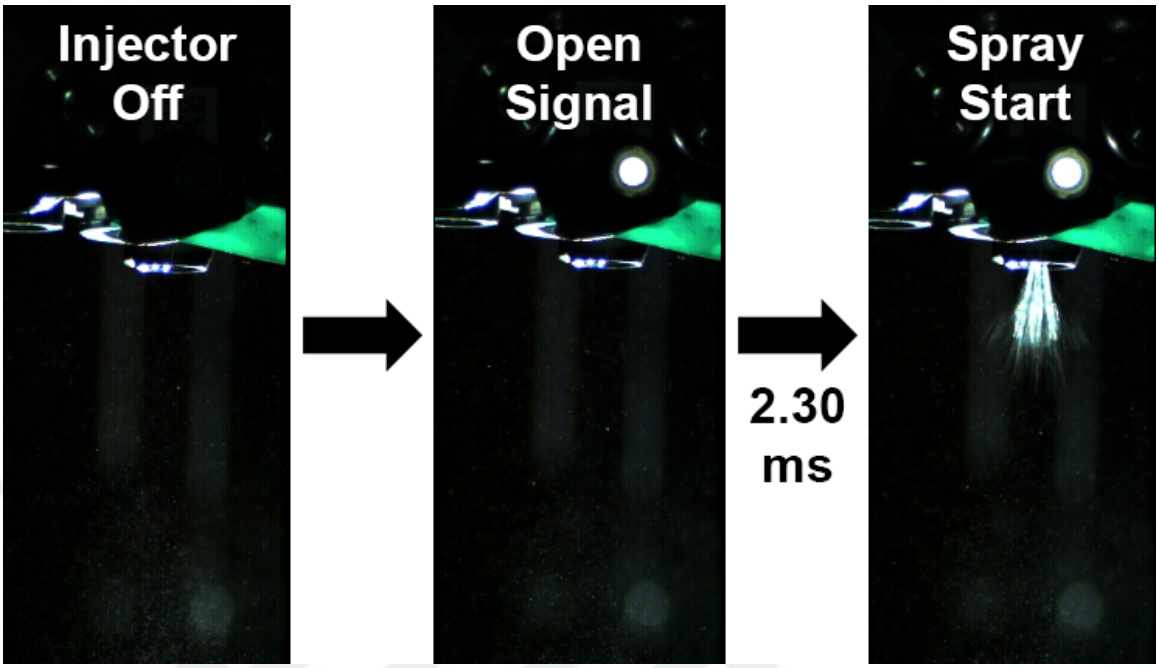

Figure 25: High speed camera shows latency between opening signal and fluid release

Besides, current and voltage changes were measured and the opening time of the plunger needle was deducted from the current profile. To find the plunger needle's opening time, eddy current phenomenon was used. The effect of this phenomenon can be seen in Figure 26. A small drop in the current profile indicates that the needle reaches the physical limit. The reason for this drop is the change in the magnetic field caused by the zeroing of the plunger speed.

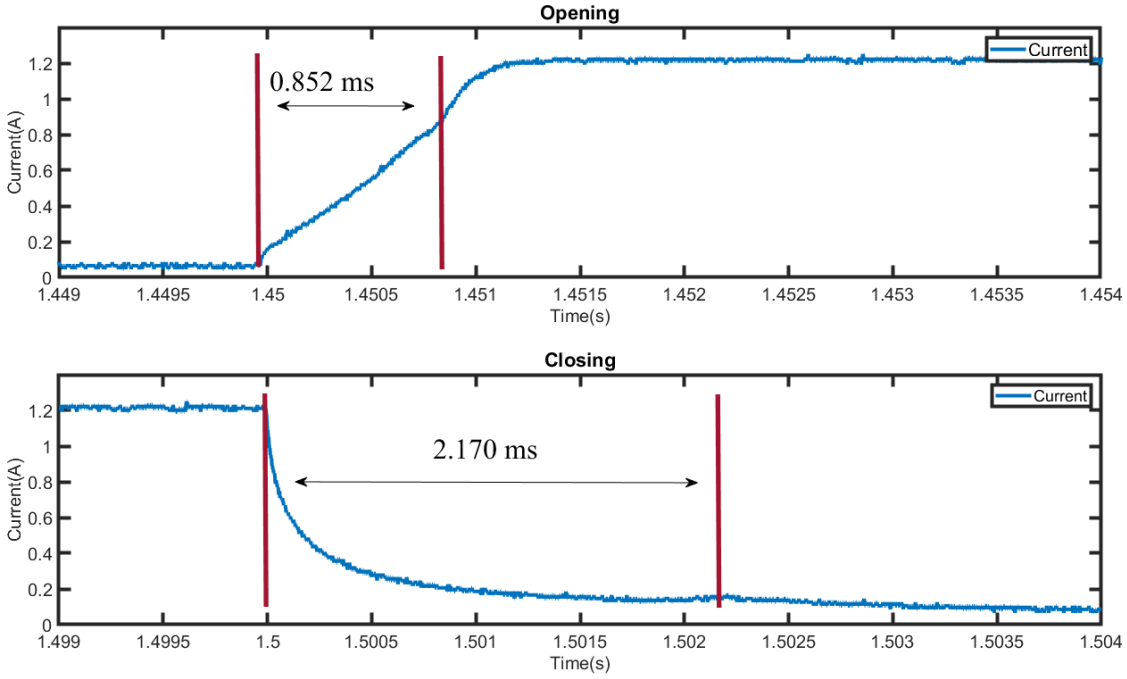

Figure 26: Opening and closing times acquired from eddy current effects. The time between vertical lines shows the duration that needs open and close injector.

Summary of these two tests can be seen in Table 5. This information is used for the calibration of the injector which is mentioned in Subsection 4.1.1.

	Opening Time	Closing Time
From Current Prob Data	0.852 ms	2.170 ms
From High Speed Camera	0.860 ms	2.300 ms
Fluid Latency	0.008 ms	0.130 ms

Table 5: Fluid latency founded by take time differences of mechanical opening and closing times and fluid observation times.

4.1.1 ECU and Urea injector

Most urea injector work with an ECU (Engine Control Unite) to spray a certain amount of urea. In vehicles, sensors are not used directly to create a closed-loop control. Injectors are actuated using open-loop control with precalibrated dosing amounts. Opening and closing time of the solenoids is determined by spray tests done before actual use. Certain duration would create a pre-measured amount of urea spray. All injectors, therefore, have to be calibrated before the actual use. Every change that is made on the injector changes the spray characteristic and ECU must be informed about the injector's characteristic accordingly. That is one of the reasons why spray latency observations are made. The duration that the injectors stayed open and the amount of liquid spray were measured to create calibration data of the OEM injector. This information was used to calibrate and compare the prototype injector that was built.

4.1.2 Peak and Hold method

Peak and Hold (P&H) method is a special voltage profile that helps to reduce power usage and keep the temperature of the solenoid low [29]. Highest power is needed during the initial opening sequence of the solenoid. Once it is opened, the required power to hold the plunger reduces significantly. In a voltage-controlled system, the given power can be controlled with PWM. The system gives full power to open and reduced power while it is open. This special PWM signal can be seen in Figure 27. Tests show there is no performance difference between on-off control and peak and hold control. But it is very important for temperature control of the solenoid actuator.

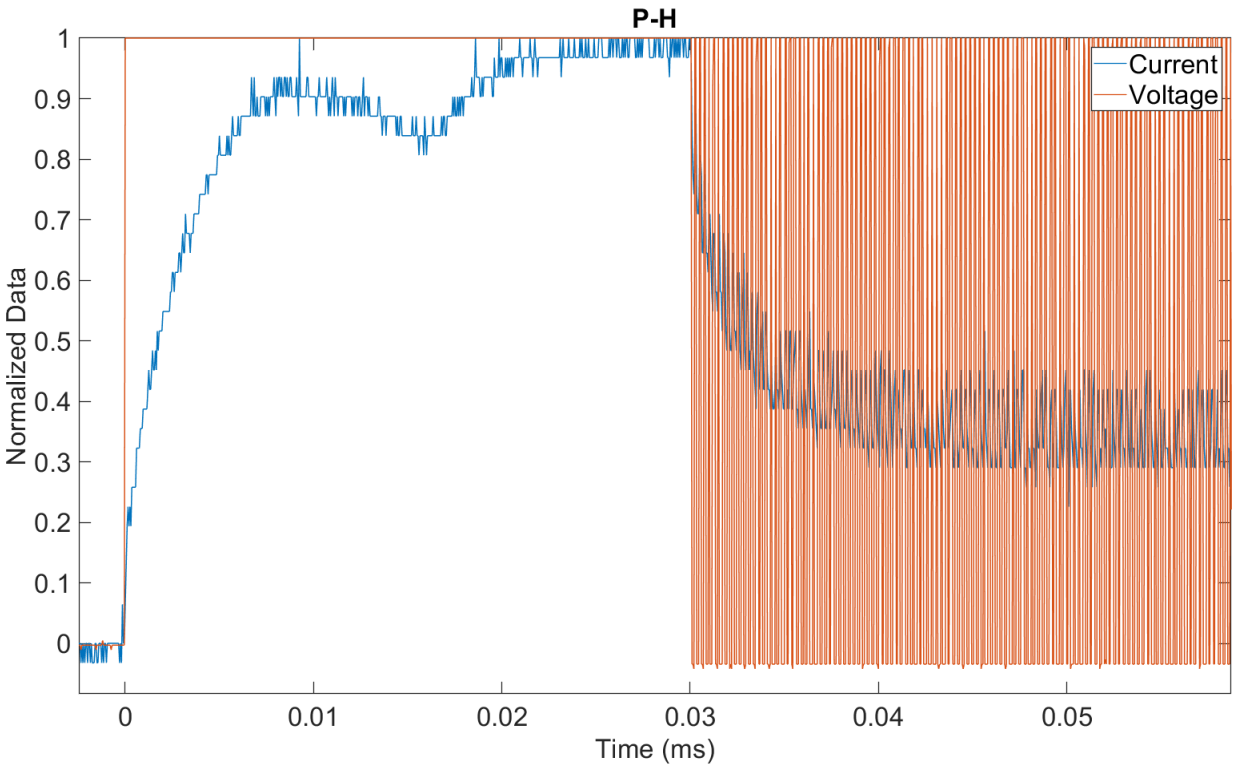

Figure 27: P&H voltage signal's effects on current can be seen on normalized data.

To better understand the temperature behavior of the solenoid actuator, a Fluke 80AK-A thermocouple was used to measure the temperature of the solenoid coil as it heats up. Two tests were conducted with two different time intervals. On the first test, a P&H signal and an on-off signal was given for 1-second and temperatures were observed. Before tests were repeated, test has been holded for the coil temperature to room temperature. On the second tests, the time interval was increased to 10 seconds and the gap between the temperature effects of P&H and the on-off signal was more pronounced. Results of these tests can be seen in Table 6.

Table 6: P&H voltage signal's temperature increments benefits can be seen on the table. For a 1 second on-off signal, the temperature rises 4.3 degree Celsius from the idle temperature. For 10 second test, this increment reaches 64 degree Celsius. With P&H signal, even for 10-second test temperature rise is 2.3 degree Celsius. The holding current given by P&H signal provide lower current to keep coil colder.

Signal Type	P&H	On-Off	P&H	On-Off
Duration	1 Seconds	1 Seconds	10 Seconds	10 Seconds
Prob Temp	24.8C	24.8C	26.8C	26.8C
Test Result	24.9C	29.1C	29.2C	64.0C
Temp Difference	0.1C	4.3C	2.3C	37.2C

4.2 Prototype Urea Injector

Using the information that was obtained from the OEM injector tests, a prototype injector was designed. More details about the design can be found in [30]. The isometric CAD view of the design can be seen in Figure 28. For designed injector, a test setup was created to observe the spraying abilities with the developed soft landing algorithm.

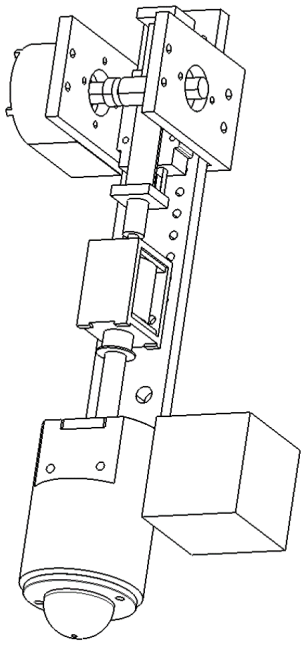

Figure 28: Prototype injector system

4.2.1 Experimental Setup for Injector Prototype

An experimental setup for injector prototype with the ability to feed pressured water to the injector system was created. The goal of this setup is to observe soft landing algorithms on an operating injector. A Broadcom HEDL-5540-A02 incremental encoder was connected to the solenoid actuator's plunger with a sliding rail system to eliminate the disturbances that could transfer from encoders tendon-capstan mechanism. This disturbance can affect needle's movement and in return, that can change injector's behaviors. This experimental system can be seen in Figure 29.

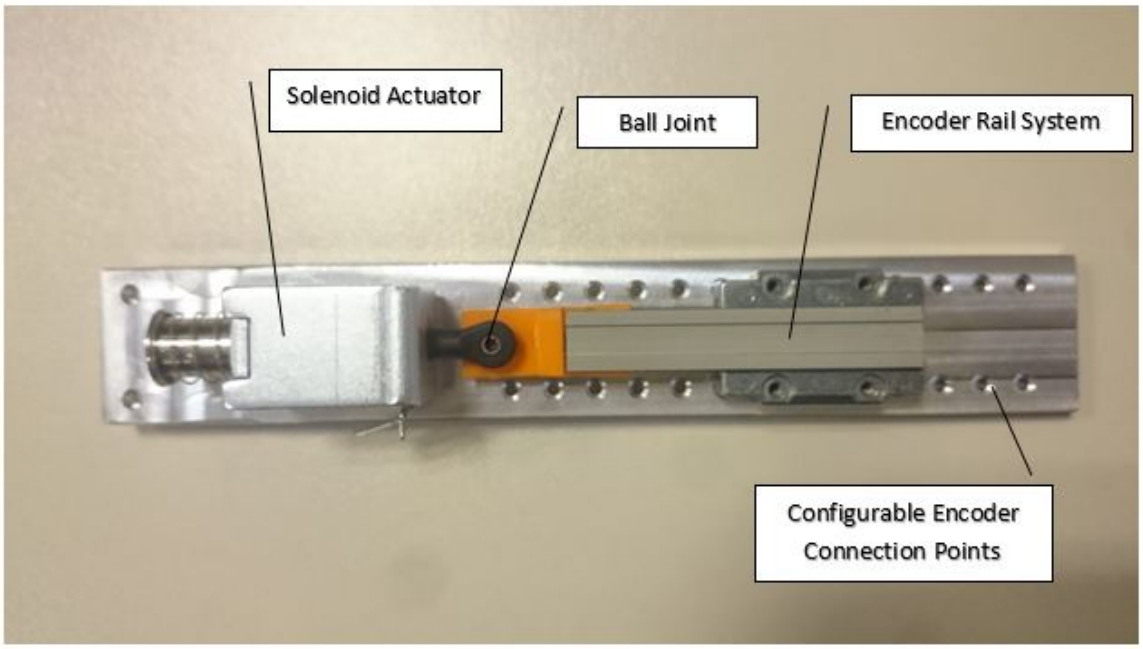

Figure 29: Encoder rail system for better alignment.

Before starting to soft landing tests, the effects of pressured water observed with a load cell that deployed of the needle. The purpose of this test is determine forces that applied to the needle from the pressure of incoming fluid because the fluid pressure can effect soft landing performance and closing times. Results of this test can be seen in Figure 30. According to results, pressure effects the needle almost ten times less than the solenoid force, so the effect of pressured water is on minimum levels and it will not prevent opening or closing action of the injector.

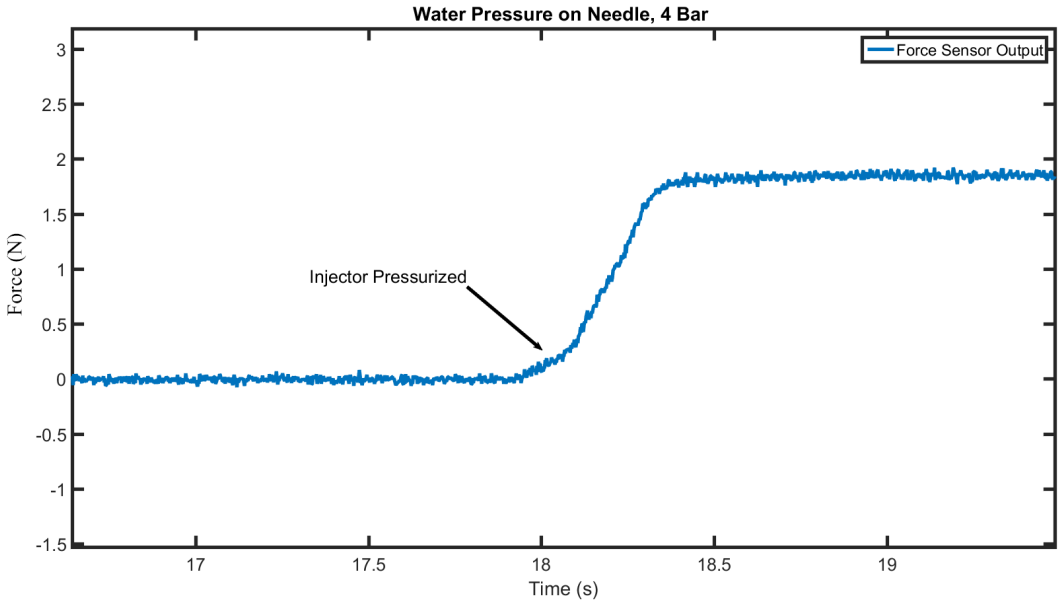

Figure 30: Force that applied by pressurized water on needle

Another issue about the test setup is short stroke distance of the needle. Although the used encoder has 0.001 mm per pulse resolution, this can cause positioning errors if used for position feedback. To check encoder's performance for moving in such small distances, a laser vibrometer sensor was used. A Polytec OFV 505 vibrometer was used which has a 0.1 picometer resolution. The validation of encoder data can be seen in Figure 30. According to results, besides a small overshot that caused by the mechanical stiffness of the encoder parts, the two sensor data overlaps, hence proving that the encoder data can be trusted for further tests.

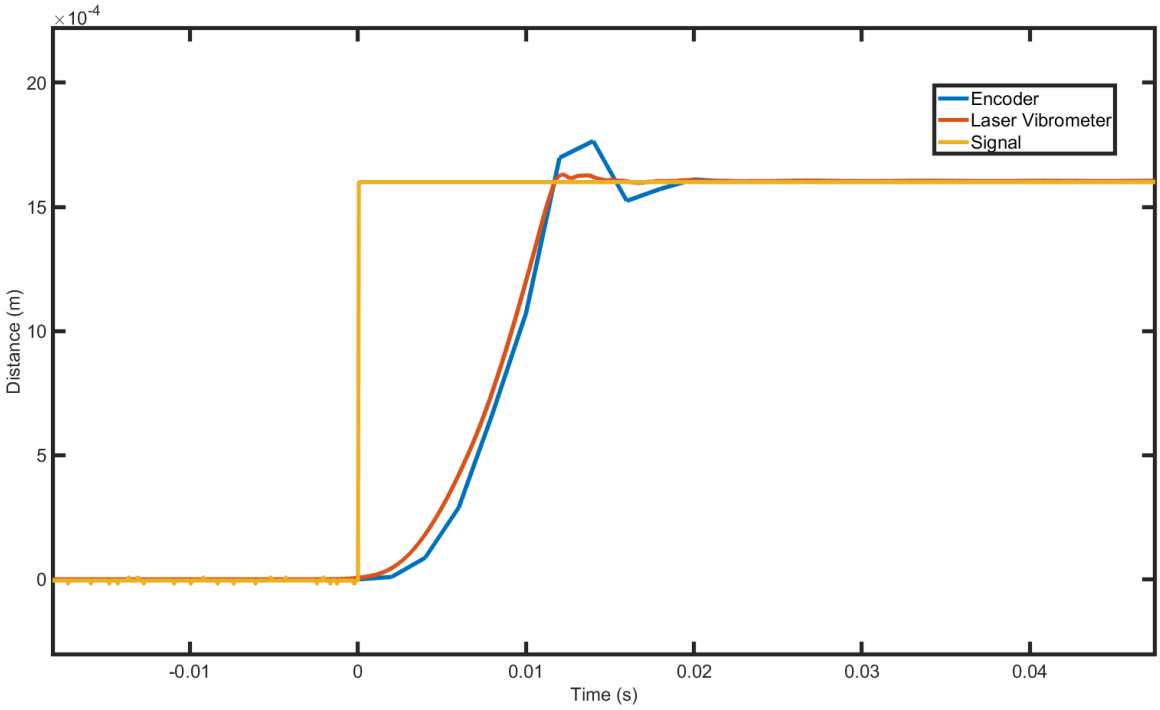

Figure 31: Comparison of laser vibrometer position data and encoder position data. Blue is the encoder data from Broadcom HEDL 5540 A02, red is the laser vibrometer data from Polytec OFV 505.

After validating the encoder's output was validated, injector input was connected to a pressurized water system. Assembled version of prototype injector for the tests can be seen in Figure 32.

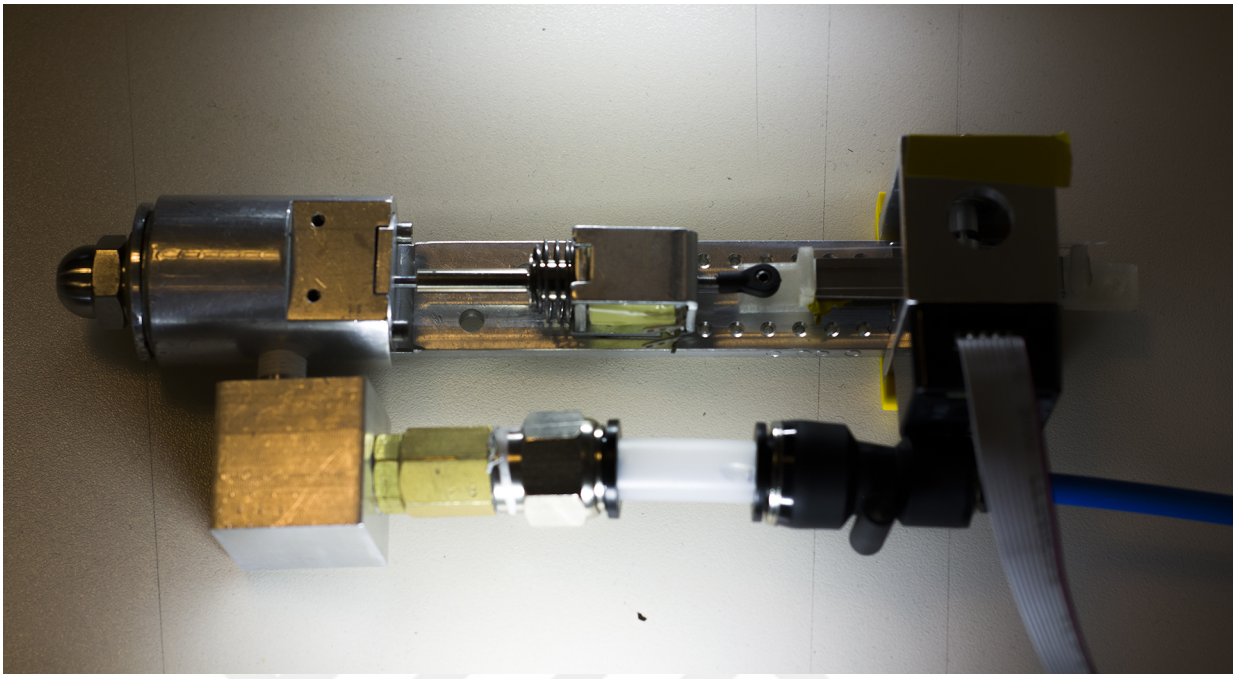

Figure 32: Prototype urea injector. Fluid is connected to the system for spray tests.

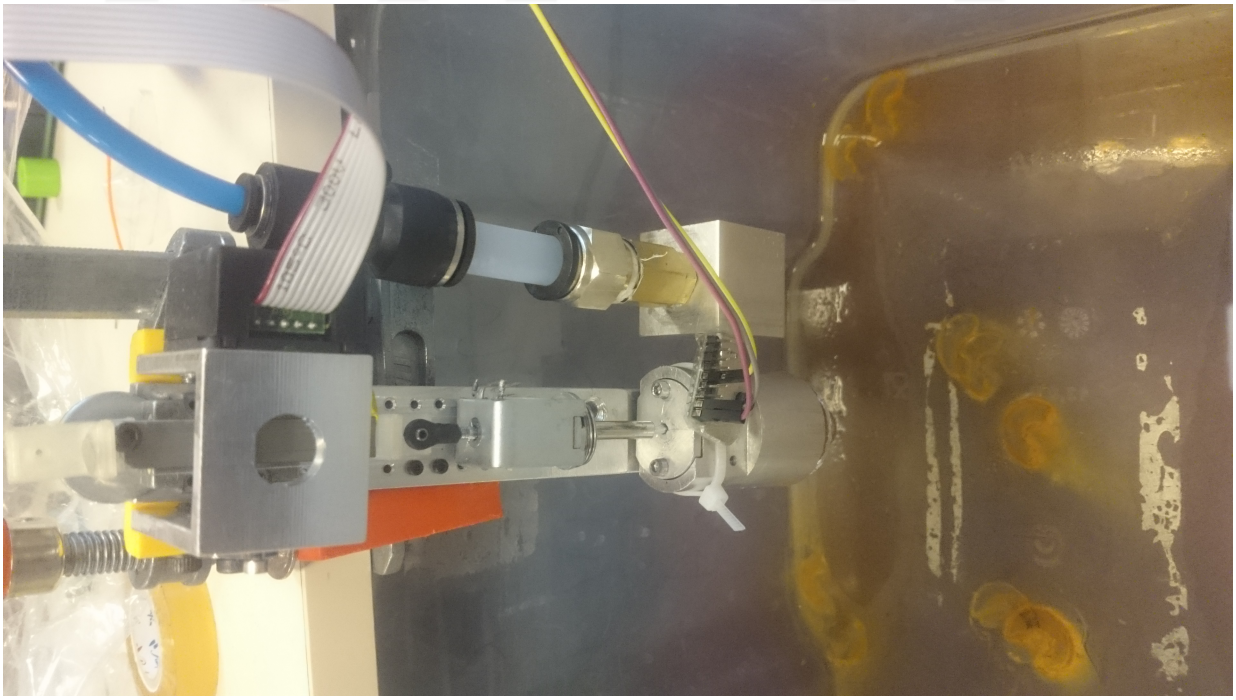

Figure 33: Test setup for soft landing with pressurized water. Water collected by plastic container

4.3 Results

Soft landing was achieved on a prototype injector with closed-loop sliding mode controller. The reference signal and tracking data can be seen in Figure 34. The reference signal in the Figure was chosen for its efficiency, which was shown in the previous soft landing test results. Only the duration of the closing ramp was shortened to 50 ms to improve the performance of the injector system.

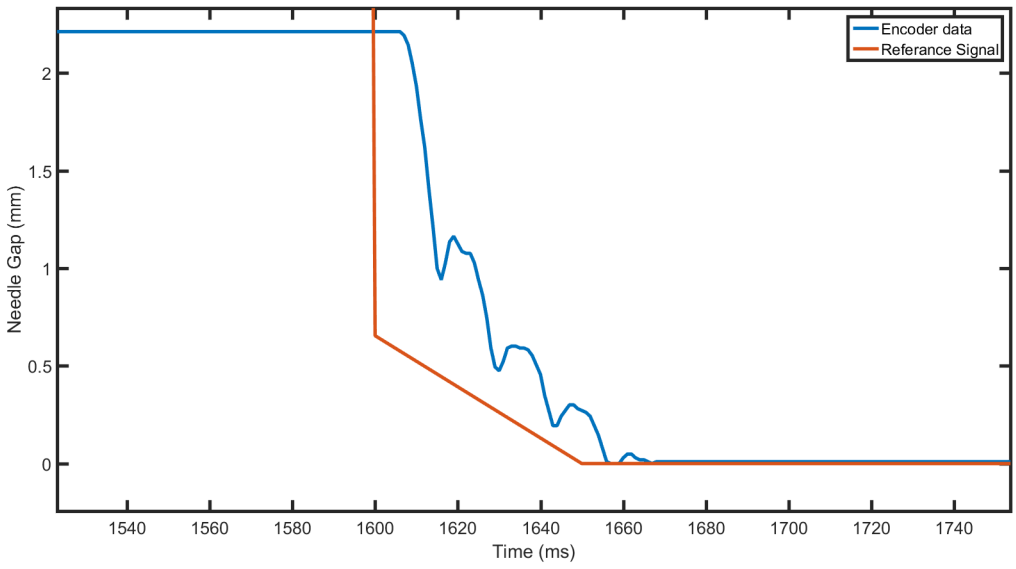

Figure 34: Test results for soft landing with pressurized water. Prototype injector shown in Figure 32 was used for the tests.

The same simulation that was explained in the previous chapter was used to test the response of the new prototype. However due to the unmodelled fluid dynamics and changes in the mechanical structures of the injector the simulation failed to imitate the real system. Since it is not always efficient to test the injector with a high-pressure fluid, it was essential to develop a new simulation with an inclusive pressurized fluid model. To solve the issue, Matlab Simulink's system identification

toolbox was used to create a model of the system. This tool adapted the non-linear structure of the injector system and provided a transfer function as its output. Flow chart of system identification's training process can be seen in Figure 36. When the created transfer function was used in the simulated alongside the actual system with the same input, the simulation provided very close results to the real test setup. Therefore, the tested non-linear transfer function was used as an observer in the open-loop controller. Simulation output with the new system model can be seen in Figure 35 along with encoder data and the reference signal.

With the trained transfer function, the controller achieved soft landing without encoder input. It provided faster experiments for tuning controller without the need for a high-pressure test setup. Flow chart of open-loop control scheme using the simulated encoder data can be seen in Figure 37.

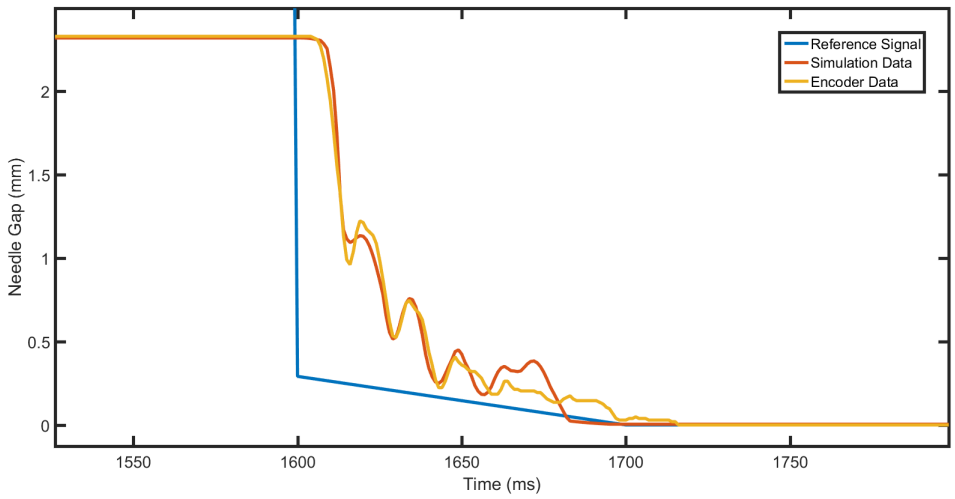

Figure 35: Encoder and simulation data with reference signal. Results shows that simulation can mimic the physical system successfully

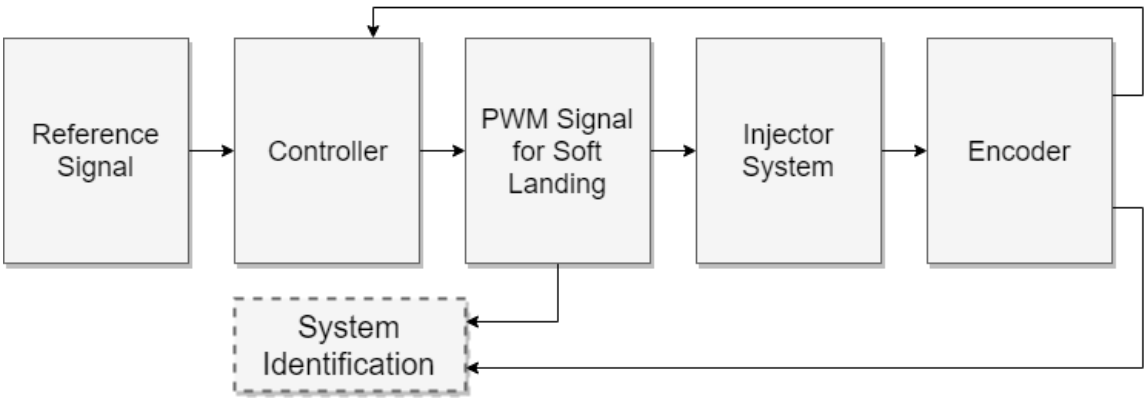

Figure 36: Training of system identification tool. PWM signal and encoder data used for train system identification.

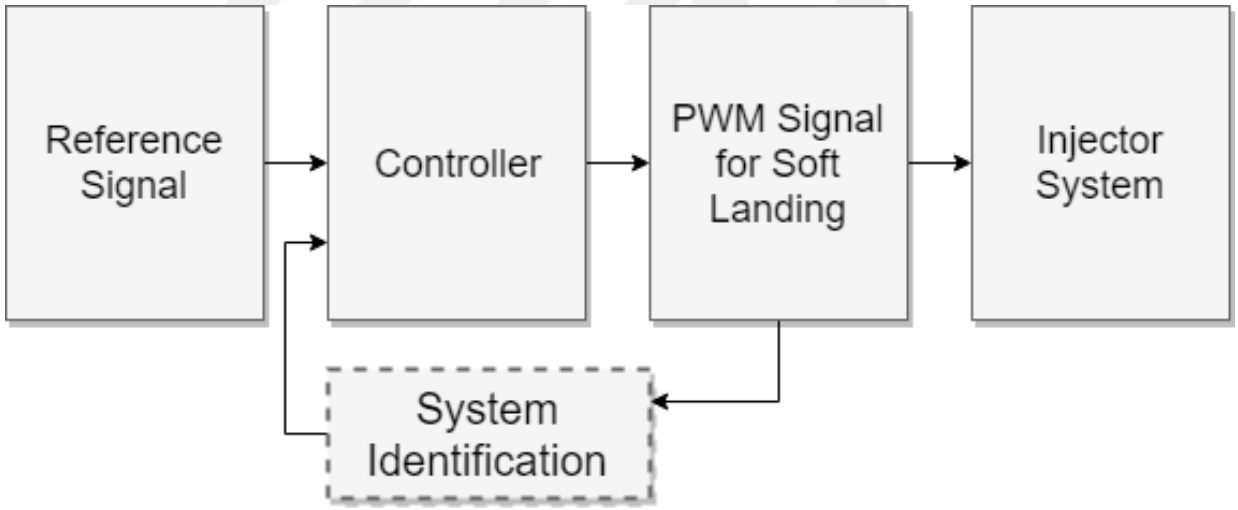

Figure 37: System works without encoder data. The position data taken from transfer function's output.

CHAPTER V

CONCLUSION

In this thesis, soft landing for a selective catalytic reduction system's urea injector was studied. A simulation model for a solenoid actuator was created using physical and magnetic parameters of the real actuator. Test setups were created to get parameters that needed for simulation. Experimental test setup for soft landing performed with controllers similar to ECU systems that are used for urea injector systems to reduce NO_x emission. PID and SMC controllers were compared for soft landing and SMC controller prove it's robustness on non-linear systems like solenoid actuators. SMC controller was able to track the reference position with minimum RMS values and lower impact velocities, unlike the PID controller.

Before the production of the prototype injector, an OEM injector was observed to understand its fluid spraying abilities and solenoid actuator's operation. The effect of fluid pressure required more complex observer for injector simulation with liquids. To do that, a new model from Simulink system identification toolbox was established by using the experimental data.Furthermore, these observations show that the ability of the injector to spray the correct amount of urea highly depended on the opening and closing times. This changed our approach for soft landing tests for the prototype injector. The reference profiles for soft landing was shortened to its minimum level to keep closing time brief. In conclusion, the solenoid actuators that used in urea injectors has nonlinear and uncertain behavior and that makes difficult to model or control them. With the help of SMC soft landing was achieved on the prototype urea injector.

Bibliography

[1] J. van Dam, B. Gysen, E. Lomonova, and M. Dhaens, "Soft-landing control of low-energy solenoid valve actuators," in *Ecological Vehicles and Renewable Energies (EVER), 2018 Thirteenth International Conference on*, pp. 1–5, IEEE, 2018.

[2] K. S. Peterson and A. G. Stefanopoulou, "Extremum seeking control for soft landing of an electromechanical valve actuator," *Automatica*, vol. 40, no. 6, pp. 1063–1069, 2004.

[3] F. Meng, H. Zhang, D. Cao, and H. Chen, "System modeling and pressure control of a clutch actuator for heavy-duty automatic transmission systems," *IEEE Transactions on Vehicular Technology*, vol. 65, no. 7, pp. 4865–4874, 2016.

[4] G. Schaller and H. Hofmann, "Electromechanical shift device for a change-speed gearbox of a motor vehicle," May 23 2000. US Patent 6,065,363.

[5] J. D. Ervin, B. A. Boyer, G. P. McConville, and K. H. Ku, "Method for controlling vibrations during transitions in a variable displacement engine," Jan. 23 2018. US Patent 9,874,166.

[6] J.-L. Gastineau, S. Durand, and A. Gennesseaux, "Method of damping vibration, active hydraulic anti-vibration mount and vehicle including such a mount," Feb. 25 2003. US Patent 6,523,816.

[7] H. G. Havard, R. Goel, R. M. Leal, T. E. Pate, *et al.*, "Solenoid control methods for dual flow hvac systems," Feb. 6 2018. US Patent 9,884,394.

[8] R. C. Bussjager, J. M. McKallip, and L. N. Miller, "High latent refrigerant control circuit for air conditioning system," Apr. 22 1997. US Patent 5,622,057.

[9] T. Denton, *Automobile electrical and electronic systems*. Routledge, 2017.

[10] C. E. Pettit, "Locking gas cap system," June 21 1977. US Patent 4,030,322.

[11] Y. Jiang, J. Zhao, J. Duan, H. Hao, and M. Wang, "Automatic control system of water and fertilizer based on fuzzy control algorithm and simulation," in *Technology, Networking, Electronic and Automation Control Conference (ITNEC), 2017 IEEE 2nd Information*, pp. 1671–1674, IEEE, 2017.

[12] G. A. Sims, "Integrated pest control system," July 31 1990. US Patent 4,944,110.

[13] B. D. Egley and P. S. James, "Dialysis control valve having self-cleaning mode," June 2 2015. US Patent 9,044,586.

[14] E. Sideris, C. Georgiou, M. Koupparis, and P. Macheras, "Automated flow-injection serial dynamic dialysis technique in the study of drug binding with cyclodextrins," *Analytica chimica acta*, vol. 289, no. 1, pp. 87–95, 1994.

[15] D. V. Prabu, A. Sathishkumar, C. Manibalaji, T. Sakthivel, and V. Robin, "Accurate position control of pneumatic actuator using on/off solenoid valve," 2017.

[16] R. B. Van Varseveld and G. M. Bone, "Accurate position control of a pneumatic actuator using on/off solenoid valves," *IEEE/ASME Transactions on mechatronics*, vol. 2, no. 3, pp. 195–204, 1997.

[17] T. V. Johnson, "Diesel emission control in review," *SAE International Journal of Fuels and Lubricants*, vol. 1, no. 1, pp. 68–81, 2009.

[18] R. R. Chladny and C. R. Koch, "Flatness-based tracking of an electromechanical vvt actuator with magnetic flux sensor," in *2006 IEEE Conference on Computer Aided Control System Design, 2006 IEEE International Conference on Control Applications, 2006 IEEE International Symposium on Intelligent Control*, pp. 1663–1668, Oct 2006.

[19] W. Hoffmann, K. Peterson, and A. G. Stefanopoulou, "Iterative learning control for soft landing of electromechanical valve actuator in camless engines," *IEEE Transactions on Control Systems Technology*, vol. 11, pp. 174–184, March 2003.

[20] K. S. Peterson and A. G. Stefanopoulou, "Extremum seeking control for soft landing of an electromechanical valve actuator," *Automatica*, vol. 40, no. 6, pp. 1063 – 1069, 2004.

[21] R. R. Chladny and C. R. Koch, "Flatness-based tracking of an electromechanical variable valve timing actuator with disturbance observer feedforward compensation," *IEEE Transactions on Control Systems Technology*, vol. 16, pp. 652–663, July 2008.

[22] A. Gaeta, C. I. Hoyos Velasco, and U. Montanaro, "Cycle-by-cycle adaptive force compensation for the soft-landing control of an electro-mechanical engine valve actuator," *Asian Journal of Control*, vol. 17, no. 5, pp. 1707–1724, 2015.

[23] W. Hoffmann, K. Peterson, and A. G. Stefanopoulou, "Iterative learning control for soft landing of electromechanical valve actuator in camless engines," *IEEE Transactions on control systems technology*, vol. 11, no. 2, pp. 174–184, 2003.

[24] P. Oxley, J. Goodell, and R. Molt, "Magnetic properties of stainless steels at room and cryogenic temperatures," *Journal of Magnetism and Magnetic Materials - J MAGN MAGN MATER*, vol. 321, pp. 2107–2114, 07 2009.

[25] K. J. Åström and T. Hägglund, *PID controllers: theory, design, and tuning*, vol. 2. Instrument society of America Research Triangle Park, NC, 1995.

[26] A. Bartoszewicz and R. J. Patton, "Sliding mode control," *International Journal of Adaptive Control and Signal Processing*, vol. 21, no. 8-9, pp. 635–637, 2007.

[27] V. Utkin, J. Guldner, and J. Shi, *Sliding mode control in electro-mechanical systems*. CRC press, 2017.

[28] A. Levant, "Sliding order and sliding accuracy in sliding mode control," *International journal of control*, vol. 58, no. 6, pp. 1247–1263, 1993.

[29] F. Breidi, T. Helmus, and J. Lumkes, "The impact of peak-and-hold and reverse current solenoid driving strategies on the dynamic performance of commercial cartridge valves in a digital pump/motor," *International Journal of Fluid Power*, vol. 17, no. 1, pp. 37–47, 2016.

[30] A. Yagcı, S. Qureshi, M. Kuntuz, and O. Bebek, "Design of a solenoid based prototype injector for evaluation of electromagnetic parameters," in *19th International Symposium on Electromagnetic Fields in Mechatronics, Electrical and Electronic Engineering*, Aug 2019.

VITA

Mehmet Polat KÜNTÜZ received his bachelor's degree in electric and electronic engineering from Özyeğin Üniversity in 2015. He has been pursuing his MSc degree in mechanical engineering under the supervision of Dr. Bebek at the robotics lab.